

Review

Recent Advances in Black TiO₂ Nanomaterials for Solar Energy Conversion

Lijun Liao [†], Mingtao Wang [†], Zhenzi Li , Xuepeng Wang ^{*} and Wei Zhou ^{*} 

Shandong Provincial Key Laboratory of Molecular Engineering, School of Chemistry and Chemical Engineering, Qilu University of Technology (Shandong Academy of Sciences), Jinan 250353, China

^{*} Correspondence: wxpchem@hotmail.com (X.W.); wzhou@qlu.edu.cn (W.Z.)

[†] These authors contributed equally to this work.

Abstract: Titanium dioxide (TiO₂) nanomaterials have been widely used in photocatalytic energy conversion and environmental remediation due to their advantages of low cost, chemical stability, and relatively high photo-activity. However, applications of TiO₂ have been restricted in the ultra-violet range because of the wide band gap. Broadening the light absorption of TiO₂ nanomaterials is an efficient way to improve the photocatalytic activity. Thus, black TiO₂ with extended light response range in the visible light and even near infrared light has been extensively exploited as efficient photocatalysts in the last decade. This review represents an attempt to conclude the recent developments in black TiO₂ nanomaterials synthesized by modified treatment, which presented different structure, morphological features, reduced band gap, and enhanced solar energy harvesting efficiency. Special emphasis has been given to the newly developed synthetic methods, porous black TiO₂, and the approaches for further improving the photocatalytic activity of black TiO₂. Various black TiO₂, doped black TiO₂, metal-loaded black TiO₂ and black TiO₂ heterojunction photocatalysts, and their photocatalytic applications and mechanisms in the field of energy and environment are summarized in this review, to provide useful insights and new ideas in the related field.

Keywords: photocatalysis; black TiO₂; doping; heterojunction; solar energy conversion



Citation: Liao, L.; Wang, M.; Li, Z.; Wang, X.; Zhou, W. Recent Advances in Black TiO₂ Nanomaterials for Solar Energy Conversion. *Nanomaterials* **2023**, *13*, 468. <https://doi.org/10.3390/nano13030468>

Academic Editor: Chiara Maccato

Received: 29 December 2022

Revised: 16 January 2023

Accepted: 21 January 2023

Published: 24 January 2023



Copyright: © 2023 by the authors. Licensee MDPI, Basel, Switzerland. This article is an open access article distributed under the terms and conditions of the Creative Commons Attribution (CC BY) license (<https://creativecommons.org/licenses/by/4.0/>).

1. Introduction

With the rapid development of industry and human society, fossil fuels, including coal, natural gas, and petroleum, have been excessively consumed in the last decades, thereby creating energy crises and environmental pollutions. Searching for alternative energy resources and improving the living environment have become urgent issues all over the world. Photocatalytic technology, which can employ the inexhaustible solar energy to H₂ generation from water splitting [1–3], CO₂ reduction to small sustainable fuels [4–6], and environmental pollutant degradation [7–9], has been developed and attracted much attention due to a series of excellent physical and chemical characteristics, such as low energy consumption, simple operation, no secondary pollution, low cost, and sustainability [10]. Since 1972, TiO₂ has been used as a photocatalyst and developed rapidly in the field of energy conversion and environmental remediation [1]. Three main kinds of TiO₂, including anatase, rutile, and brookite, can be distinguished according to their different crystal structures [11–13]. Anatase and rutile are the most frequently investigated TiO₂ photocatalysts because of their superior photocatalytic activity under UV irradiation than brookite. The photocatalytic performance and properties of TiO₂ are severely influenced by its preparation, morphology, and dimensions. Serga et al. reported an extraction-pyrolytic method for the synthesis of nanocrystalline TiO₂ powders using valeric acid as an extractant [14]. This method can be applied for the fabrication of anatase, rutile, or mixed anatase-rutile TiO₂ powders [14]. Poly (titanium dioxide) is found to have a significant influence on the component compatibility and relaxation behavior of

interpenetrating polymer networks [15]. TiO₂ photocatalysts treated at 800 °C in hydrogen atmosphere for 1 h showed higher visible photocatalytic activity for C-H/C-H coupling of dipyrromethanes with azines than commercial TiO₂ (P25) [16]. TiO₂ nanosheets were proved to exhibit superior photocatalytic activity for CO₂ reduction than the nanoparticle, thanks to its much higher surface area and surface activity [17]. In addition, the effects of the particle size of TiO₂ on photocatalytic pollutant removal were thoroughly investigated by Kim et al. [18]. The photocatalytic degradation efficiency for methylene blue can be effectively improved by controlling the particle size and TiO₂ concentration in the reaction mixture [18].

However, due to the wide band gap of TiO₂ (anatase: 3.2 eV, rutile: 3.0 eV), it can only absorb the ultraviolet part of sunlight (less than 5%), resulting in low light utilization efficiency and low photocatalytic activity [19]. In addition, the high photo-generated electron-hole recombination rate of TiO₂ materials leads to low quantum efficiency [20]. Therefore, improving the quantum efficiency and photocatalytic activity have always been a concern in the field of photocatalysis.

Previously, the doping modification of TiO₂, including metal ions (such as Co, Ni, Pt, etc.) or nonmetallic ion (N, H, S, etc.), was introduced to directly modify the TiO₂ surface electronic properties and broaden the absorption of light, thus improving the efficiency of the charge separation on the TiO₂ surface [21,22]. Later, TiO₂ nanomaterials were also combined with other semiconductors to form heterojunctions, thereby enhancing the photo-induced charge separation and migration efficiency, and greatly reducing the corresponding recombination rate [23,24]. In 2011, Chen et al. reported that the hydrogenation strategy can reduce the band gap of TiO₂, change its color from white to black, expand the light response range to the visible/near infrared region, and improve the visible light catalytic performance [25]. This partially reduced TiO₂ is coined as “black TiO₂” in the study [25]. Since then, studies on black TiO₂ in various fields of photocatalysis, including energy conversion and pollutant removal, have been growing over the last decade. The above-mentioned modification methods (such as doping, heterojunction, etc.) were subsequently applied to black TiO₂ to narrow the band gap, thereby further promoting the visible light absorption and charge separation efficiency.

In this review, the structure properties, synthesis routes, and applications of black TiO₂-based nanomaterials in the environmental and energy fields, such as photocatalytic water splitting and the photodegradation of organic pollutants, are summarized. As shown in Figure 1, the above aspects will be concluded and discussed from the perspectives of black TiO₂, doped black TiO₂, metal-loaded black TiO₂, and black TiO₂ heterojunction. Finally, the status quo of black TiO₂ materials is reviewed, and the future development prospects and challenges are proposed.

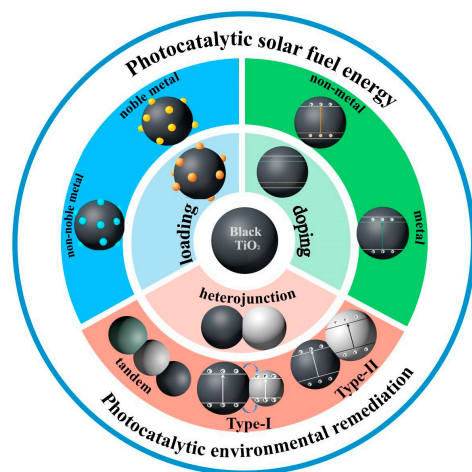


Figure 1. Outline diagram of the types of black TiO₂ nanomaterials.

2. Morphology and Structural Properties of Black TiO₂

The beauty of nanomaterials is that the (photo)catalytic activity is highly influenced by their morphology and structural properties, including the crystal structure, presence of vacancies, and partially phase transformation. Scanning electron microscopy (SEM) and transmission electron microscopy (TEM) were frequently utilized to investigate the morphology of black TiO₂. Black TiO₂ with different morphologies, such as nanospheres [26–34], nanotubes [35–38], nanoarrays [39–43], nanowires [44–47], nanoplates [48,49], nanosheets [50,51], nanobelts [52,53], nanocages [54], nanoflowers [55], nanofibers [56], hollow shells [57–59], films [60,61], and nanolaces [62], were synthesized via varied synthetic approaches. Commercial TiO₂ materials are often directly used to produce black TiO₂ nanospheres. Biswas et al. obtained black TiO_{2-x} nanoparticles at high temperatures via NaBH₄ reduction and studied their light absorption ability after reduction [28]. The band gap of black TiO₂ nanospheres was 2.54 eV, which was much lower than the pristine commercial anatase (3.27 eV) [28]. Katal et al. prepared black TiO₂ nanoparticles at high temperatures under a vacuum atmosphere and investigated the color change and shrinkage of reduced TiO₂ pellets over temperature [63]. The reduction process was performed by sintering commercial P25 pellets under a vacuum condition at different temperatures (500, 600, 700, 800 °C) for 3 h [63]. The color of the white P25 pellets changed into pale yellow after calcination at 500 °C in the air condition [63]. Its color became darker after sintering at 500 °C under the vacuum condition [63]. Black TiO₂ pellets were obtained after calcination at temperatures higher than 500 °C, and the size of the pellets became smaller after treatment at 700 °C [63]. The phase transformation from anatase to rutile was observed in TiO₂ after high temperature calcination [63]. The corresponding visible change and red-shift in UV-vis absorption spectra are presented in Figure 2A [63]. The band gap energy gradually decreased with temperature from 3.1 eV for P25, to 2.24 eV for BT-800 [63].

The synthesis of black TiO₂ with unique morphology, such as nanoflowers, tubes, and wires, usually necessitates specific synthetic procedure for TiO₂ nanomaterials, including hydrothermal, solvothermal treatment, anodization, etc. Lim et al. prepared partially reduced hollow TiO₂ nanowires (R-HTNWs) using the hydrothermal method and the subsequent treatment with NaBH₄ under the nitrogen atmosphere [47]. The local distribution of Ti³⁺ species (oxygen vacancies) in reduced hollow TiO₂ nanowires was confirmed to be primarily present in the surface region compared to the core using electron energy loss spectroscopy (EELS) [47]. In addition, trace impurities including B, Na, N from NaBH₄, and nitrogen were located mostly at the surface and the distorted rutile structure region of R-HTNWs [47]. The SEM, TEM image, and EELS Ti L_{2,3} data are illustrated in Figure 2B [47]. Ti³⁺ present on the surface of TiO₂ could be stabilized by the surface impurities [47]. Black TiO₂ materials generally possessed certain amounts of oxygen vacancies, which can be confirmed by X-ray photoelectron spectroscopy (XPS). The concentration of oxygen vacancies was normally controlled by the different thermal treatment time or temperature [41,45,51]. However, there is lack of precise, quantitative characterization techniques for oxygen vacancies present on the black TiO₂ surface. The band gap parameters of black TiO₂ were usually measured and calculated by XPS and UV-vis spectroscopy measurements. The decrease in E_g of black TiO₂ was assumed to be related to the surface disorder, including the presence of Ti³⁺ and oxygen vacancies [47].

The mesoporous structure of TiO₂ can increase the surface area and phase stability. Zhou et al. synthesized mesoporous black TiO₂ hollow spheres (MBTHSs) via the combination of a template-free solvothermal method and amine molecules encircling strategy, and the subsequent atmospheric hydrogenation process [64]. The wall thickness and diameter of MBTHSs could be tuned by adjusting the solvothermal reaction time and the Ti precursor concentration, respectively [64]. Ti³⁺ species were proved to be mainly present in the bulk but not on the surface of MBTHSs via XPS

measurements [64]. The light absorption of MBTHSs was effectively extended to the visible light range compared with the pristine TiO₂ [64]. The synthetic procedure, SEM image, and UV-vis absorption properties are present in Figure 2C [64]. The anatase phase remained unchanged after hydrogenation [64]. The band gap of mesoporous TiO₂ was largely reduced to 2.59 eV after hydrogenation [64]. The black TiO₂ consisted of mesoporous structure with cylindrical channels providing the relatively high surface area of ~124 m² g⁻¹ [64]. They also fabricated the heterojunctions of γ -Fe₂O₃ nanosheets/mesoporous black TiO₂ hollow sphere to enhance the charge separation and photocatalytic tetracycline degradation efficiency [59]. Porous black TiO₂ photocatalysts tended to appear in three dimensional structures, such as foams, pillars, and hollow structures. Zhang et al. synthesized the 3D macro-mesoporous black TiO₂ foams via freeze-drying, cast molding technology, and high-temperature surface hydrogenation [65]. The large, closed pores were generated using polyacrylamide as the organic template, while plenty of open pores were formed in the frameworks and on the surface of the black TiO₂ thanks to the water evaporation in the freeze-drying process [65]. This black TiO₂ material exhibited a self-floating amphiphilic property and an enhanced solar energy harvesting efficiency [65]. Zhou et al. prepared porous black TiO₂ pillars through an oil bath reaction and high-temperature hydrogenation reduction [66]. The porous structure and mesopores of black TiO₂ pillars were clearly observed by the Scanning electron microscope and transmission electron microscope [66]. The enhanced photocatalytic performance was attributed to more active surface sites offered by the porous pillar structure and the self-doped Ti³⁺ [66]. The hollow structured black TiO₂ with plenty of pore channels and an exposed surface also showed an enhanced photocatalytic efficiency [57]. The pores of the porous black TiO₂, generally located in its whole frameworks with open pores connected with surface, providing abundant active sites and surface defects, thus promoting the photocatalytic performance. Ethylenediamine was often utilized to maintain the porous structure of black TiO₂ and to prevent its phase transformation from anatase to rutile.

In addition to oxygen vacancies, disordered structures and surface amorphization in black TiO₂ may have significant impacts on its photoresponsive properties. Kang et al. prepared black TiO₂ with amorphous domains through a glycol-assisted solvothermal method and subsequent calcination [67]. Oxygen vacancies were introduced in the amorphous domains of the black TiO₂ nanosheets [67]. Figure 2D shows the color and optical absorption property changes [67]. The color of the brown TiO₂ turned into black after 2 h of calcination at 350 °C under Ar [67]. The light absorption of black TiO₂ was significantly extended to the near-infrared region [67]. Oxygen vacancies were confirmed to be present in the subsurface of black TiO₂ by first-principle calculations [67]. Table 1 summarizes the properties of some black TiO₂ nanomaterials with varied morphology. The color of most reduced TiO₂ is black. The morphology of black TiO₂ is not determined by the reduction process.

Table 1. Properties of black TiO₂ nanomaterials.

Crystal Phase	Reducing Agent	Color	Morphology	Oxygen Vacancies	Ref.
Anatase with minor rutile	NaBH ₄	Black	Nanospheres	✓	[26]
Anatase and rutile	Hydrogen radicals	Black	Nanospheres	✓	[27]
Anatase	NaBH ₄	Black	Nanoparticles	✓	[28]
Anatase and rutile	Hydrogen	Black	Microspheres	✓	[29]
Anatase and rutile	Pulsed Laser Ablation in Liquid	Black	Core-shell microspheres	✓	[30]

Table 1. Cont.

Crystal Phase	Reducing Agent	Color	Morphology	Oxygen Vacancies	Ref.
Anatase	Urea	Black	Nanoparticles	✓	[31]
Anatase	NaBH ₄	Black	Nanospheres	✓	[32]
Anatase	NaBH ₄	Black	Nanospheres	✓	[33]
Anatase	NaBH ₄	Black	Nanospheres	✓	[34]
Anatase	Electrochemical reduction	Black	Nanotubes	✓	[35]
Anatase	CaH ₂	Black	Nanotubes	✗	[36]
Anatase	Hydrogen	Black	Nanotubes	✓	[37]
Anatase	Ag particles	Black	Nanotubes	✓	[38]
Anatase with minor rutile	Electrochemical reduction	Black	Nanotubes	✓	[39]
Anatase and rutile	Electrochemical reduction	Blue and black	Nanotube arrays	N/S	[40]
Anatase and rutile	Electrochemical reduction	Dark yellow	Nanotube arrays	✓	[41]
Anatase and rutile	aluminothermic reduction	Black	Nanotubes	✓	[42]
Anatase	Electrochemical reduction	Black	Nanotube arrays	✓	[43]
Anatase	Hydrogen	Black	Nanowires	✓	[44]
Anatase	NaBH ₄	Black	Nanowires	✓	[45]
Anatase	Glycerol	Black	Nanoparticles and nanowires	✓	[46]
Rutile	NaBH ₄	N/S	Hollow nanowires	✓	[47]
Anatase	H ₂ S and SO ₂	Black	Nanoplatelets	✓	[48]
Anatase	NaBH ₄	Black	Nanoplates	✓	[49]
Anatase	Hydrogen	Black	Nanosheets	✓	[50]
Anatase	Aluminothermic reduction	Black	Nanosheet array films	✓	[51]
Anatase	Hydrogen	Black	Nanobelts	✓	[52]
Anatase	NaBH ₄	Black	Nanobelts	✓	[53]
Anatase	Hydrogen	Black	Nanocages	✓	[54]
Anatase	Hydrogen	Black	3D nanoflower	✓	[55]
Anatase and rutile	NaBH ₄	Black	Nanofiber	✓	[56]
Anatase	NaBH ₄	Black	Hollow shell	✓	[57]
Anatase	Annealing in vacuum	Black	Core-shell	✓	[58]
Anatase	Hydrogen	Black	Mesoporus hollow sphere	✓	[59]
Anatase and rutile	Electrochemical	Black	Films	✓	[60]
Anatase	H ₂ plasma treatment	Black	Mesoporous films	✓	[61]
Anatase	Hydrogen	Black	Hierarchical nanolace films	✓	[62]

Notes: N/S: not studied; ✓: yes; ✗: no.

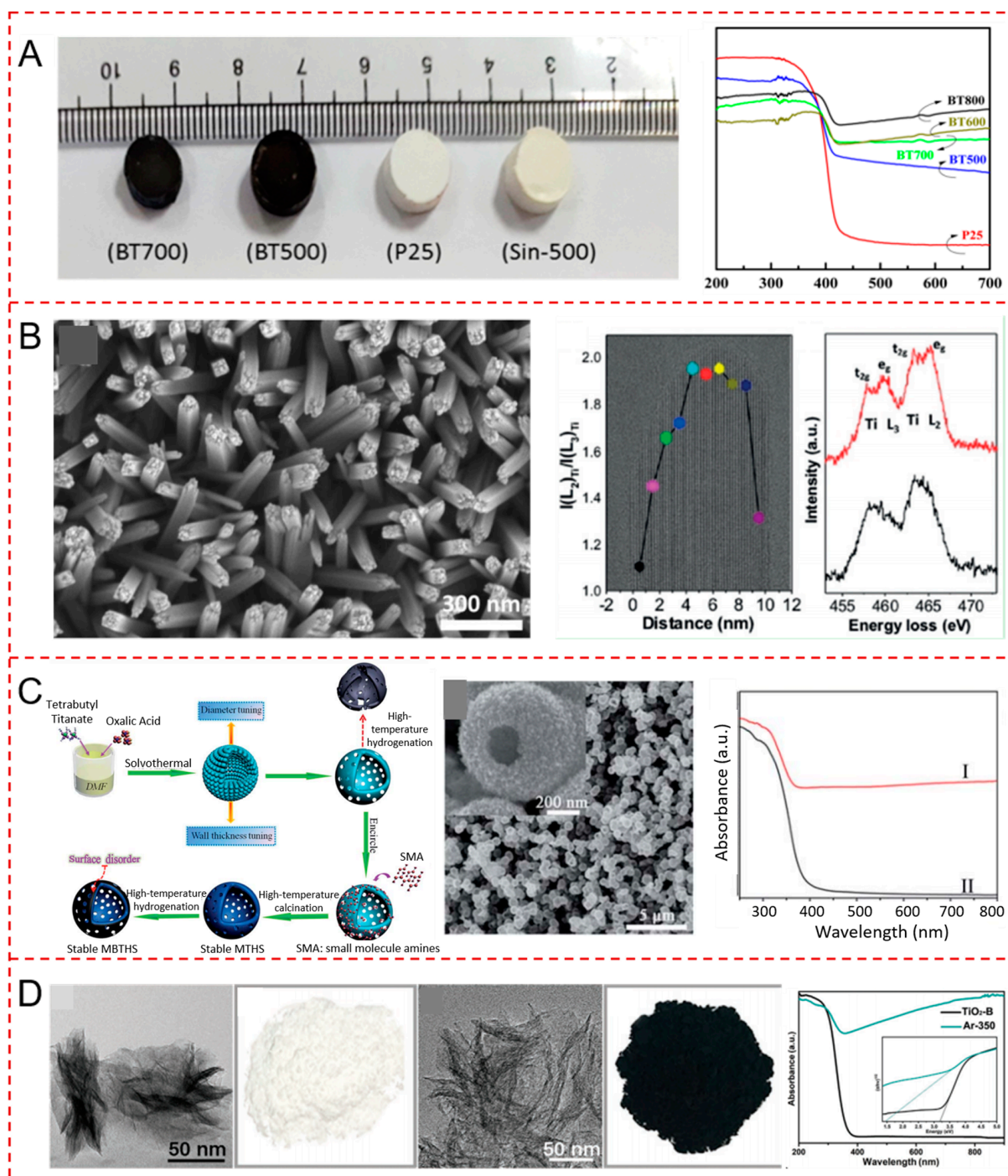
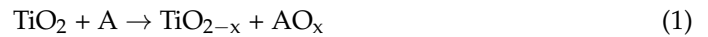


Figure 2. (A) Picture and UV-vis spectra of reduced P25 pellets at various temperatures. Reprinted with permission for ref. [63]. Copyright 2018, American Chemical Society. (B) SEM and TEM image and overlaid $I(L_{2,3})_{Ti}/I(L_3)_{Ti}$ values determined from the EELS Ti L_{2,3} data at each position of R-HTNWs. Reprinted with permission for ref. [47]. Copyright 2019, Wiley-VCH. (C) Schematic illustration of the synthetic procedure, SEM image, for MBTHSs and UV-vis absorption properties (I: mesoporous black TiO₂ hollow spheres; II: mesoporous TiO₂ hollow spheres). Reprinted with permission for ref. [64]. Copyright 2016, The Royal Society of Chemistry. (D) TEM images, and optical photographs of (black) TiO₂, and UV-vis spectra. Reprinted with permission for ref. [67] Copyright 2021, Wiley-VCH.

3. Synthesis of Black TiO₂

Currently, various methods were used to synthesize black TiO₂, which can be divided into two main approaches: high temperature hydrogenation reduction and solid phase reduction [68]. The high temperature hydrogenation method often uses hydrogen or hydrogen-contained gas mixtures to treat samples at high temperatures [69,70]. The materials used in the solid phase reduction method are generally NaBH₄ [71], CaH₂ [72], Mg powder [72], or other reducibility materials [72]. The reduction method can be expressed in reaction Equation (1):



In addition, researchers also use hot wire annealing [73], laser irradiation [74,75], anode reduction [76], and other methods to synthesize black TiO₂ [77,78].

3.1. High Temperature Hydrogenation

Hydrogen reduction involves the reduction of pure H₂ gas, H₂/Ar, or H₂/N₂ mixture at high or low pressures [69], which is a simple, effective, and straightforward method.

Zhou et al. successfully prepared the ordered mesoporous black TiO₂ material by hydrogenation at high temperature (500 °C) under atmospheric pressure (Figure 3), which had a larger specific surface area and pore size compared with the pristine titanium dioxide [79]. As shown in Figure 3, after hydrogenation at high temperature, the regular hexagonal channel of the obtained black TiO₂ was completely maintained [79]. It can be seen from the XRD in Figure 3 that there was no phase change in black TiO₂ compared with the original materials, thus proving the high thermal stability of the sample prepared by this method [79]. Notably, it can also be clearly seen that its crystallinity decreased, proved by the XRD intensity, thereby indicating that the surface disorder of TiO₂ has been created after the hydrogenation process [79]. The color of the white TiO₂ turned into black after 3 h of hydrogenation [79].

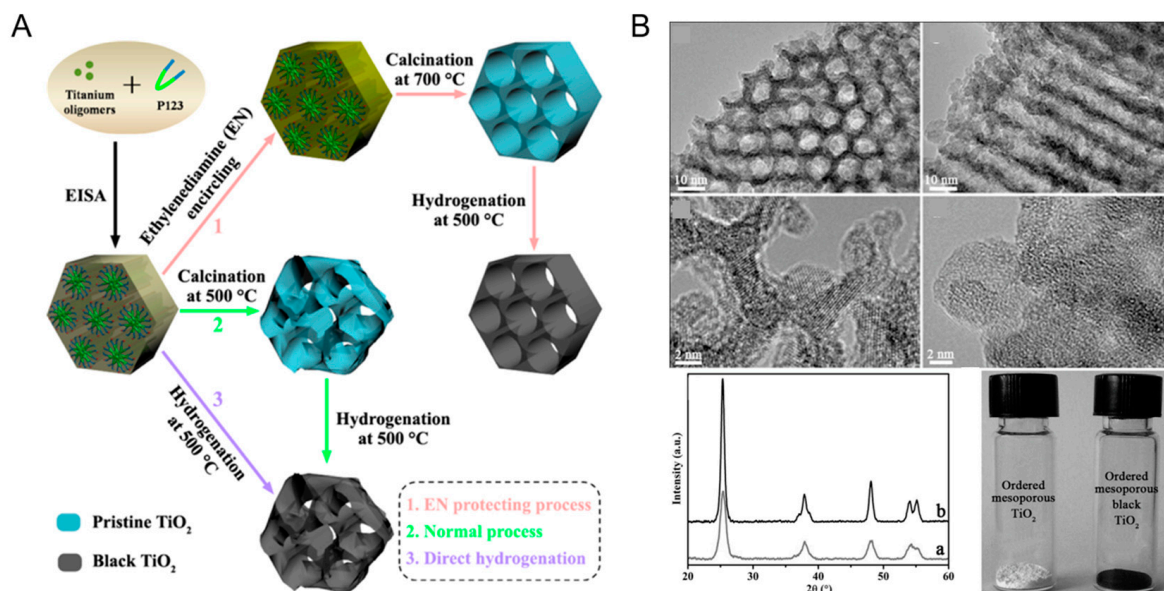


Figure 3. (A) Schematic synthesis process for the ordered mesoporous black TiO₂ materials. (B) Representative TEM images along [100] and [110] planes, HRTEM images of the ordered mesoporous black TiO₂ materials, and X-ray diffraction patterns and the photos of the ordered mesoporous black TiO₂ materials (a) and ordered mesoporous TiO₂ materials (b). Reprinted with permission for ref. [79]. Copyright 2014, American Chemical Society.

Black TiO₂ with different morphologies can be obtained via hydrogenation. Yang et al. prepared one-dimensional black TiO₂ nanotubes by the hydrogenation method, with an inner diameter of 7 nm and a wall thickness of 6 nm, as presented in Figure 4A [80].

Spherical and lamellar structures have also received much attention due to their large specific surface areas. As shown in Figure 4B, after simple hydrogenation reduction, Li et al. successfully prepared black TiO₂ nanospheres and observed the mesoporous structure in the TEM image [81]. Although the crystal surface structure of anatase became slightly disordered after hydrogenation, its special lattice fringes ($d = 0.35$ nm) did not change [81]. Black TiO₂ nanotubes with the mesoporous nanosheet structure were successfully prepared by the hydrogen reduction method by Zhang et al. [82]. Ethylenediamine coating method was used before hydrogenation [82]. The original morphology of TiO₂ was completely retained [82]. Wu et al. also synthesized two dimensional ultrathin mesoporous black TiO₂ nanosheet materials using the similar ethylenediamine encircling strategy (Figure 5) with 4 h hydrogenation reaction at 500 °C [83].

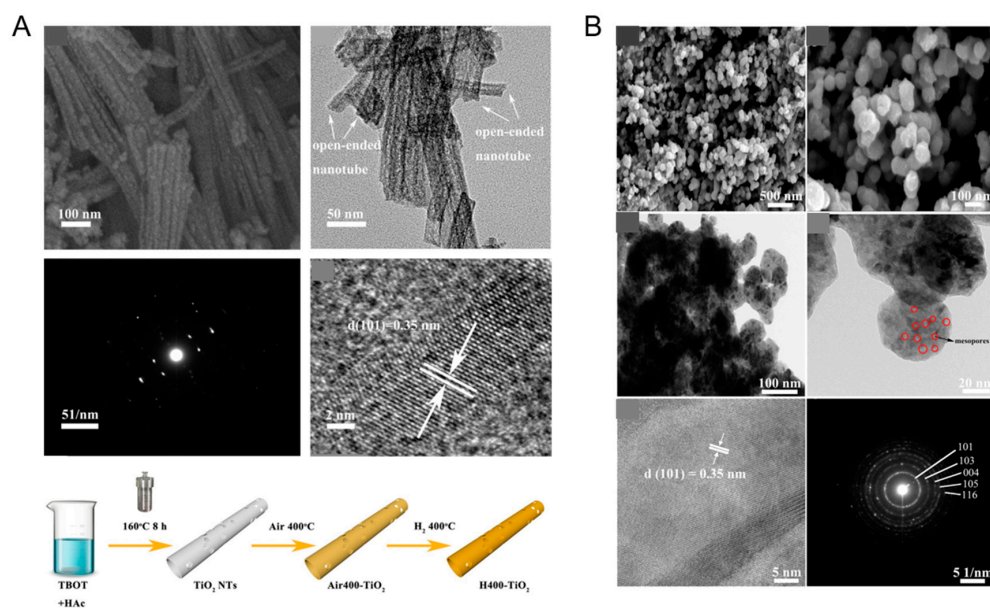


Figure 4. (A) SEM, TEM, SAED, HRTEM images and schematic illustration of the formation process of H400-TiO₂. Reprinted with permission for ref. [80]. Copyright 2021, Elsevier. (B) Representative SEM, TEM, HRTEM images and the corresponding selected area electron diffraction (SAED) pattern of the mesoporous TiO₂ nanospheres after surface hydrogenation. Reprinted with permission for ref. [81]. Copyright 2021, Elsevier.

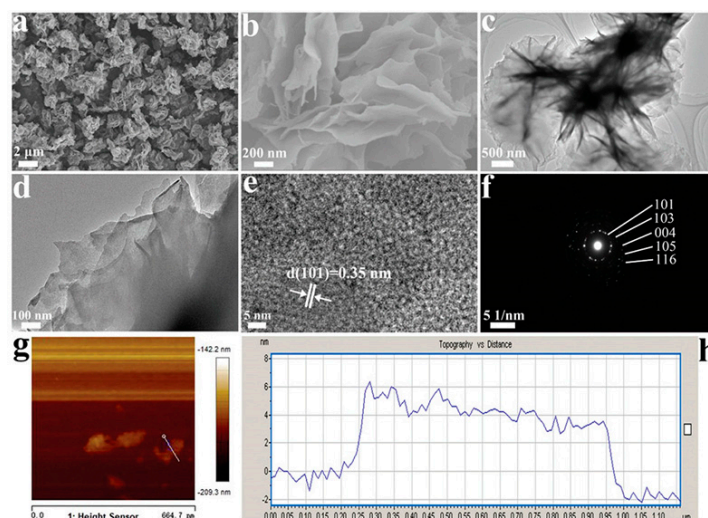


Figure 5. (a,b) SEM images, (c,d) TEM images, (e) HRTEM, (f) SAED pattern, (g) AFM topography image, and (h) the corresponding height information of the 2D ultrathin nanosheets. Reprinted with permission for ref. [83]. Copyright 2020, The Royal Society of Chemistry.

In addition to the method of hydrogen reduction at high temperature and atmospheric pressure, researchers also use the high pressure method. Wu et al. prepared black anatase TiO₂ in a two-step process [84]. The sample was degassed at 200 °C firstly, then was heated to 400 °C, and hydrogenated under high pressure (5-bar) for 24 h. The black sample was finally obtained after cooling to room temperature. The black TiO₂ was successfully prepared by Hamad et al. at a high pressure (8 bar) and relatively mild temperature [85]. The hydrogenation time was longer than in other similar research (1–5 days) [85]. The synthesized samples were uniform and stable in size, and showed higher photocatalytic activity compared with the pristine white TiO₂ [85]. Mixed gases with H₂ were also used as reducing agents in the synthesis of black TiO₂. Cai et al. successfully prepared black TiO₂ with the surface disorder structure using H₂/N₂ mixed gas with 10% content of hydrogen [86].

3.2. Solid Phase Reduction

Compared with the high temperature hydrogenation, the solid phase reduction method has certain advantages. The high temperature hydrogenation process normally starts from the outside to the inside with a relatively moderate reaction rate, while the solid phase reduction method can provide a more complete and intense reaction and may produce a series of doping at the same time. The defect is a double-edged sword. Too many defects may be detrimental to the photocatalytic performance, so the proportion and dosage of reductants in solid phase reactions should be reasonably controlled.

Xiao et al. prepared the black TiO₂ by the solid-state chemical reduction strategy by mixing the sample with sodium borohydride in a certain proportion [87]. Then, the mixture was heated in a tubular furnace with N₂ atmosphere [87]. Finally, the resulting sample was washed with deionized water to remove the unreacted sodium borohydride [87]. As shown in Figure 6, the color of the sample was getting darker with the temperature [87]. The absorption of the visible light was much enhanced after the reduction of TiO₂ [87].

Zhu et al. showed that CaH₂ can also be used as a constant reducing agent to prepare black TiO₂ [88]. The reduction process was conducted at varied temperatures [88]. It was found that the obtained black TiO₂ after reduction treatment at 400 °C had the best absorption of sunlight (over 80%), which was 11 times that of the pristine TiO₂ [88]. This simple method provides an alternative for improving the absorption of visible light on the TiO₂ surface.

Sinhamahapatra et al. reported the reduction of TiO₂ particles to black TiO₂ by magnesium thermal reduction method, which was inspired by the Kroll process, for the first time [89]. The synthetic procedure of this method was approximately identical to the method of sodium borohydride reduction [89]. TiO₂ and magnesium powder were thoroughly mixed first, and then heated in a tube furnace at 650 °C with 5% H₂/Ar for 5 h [89]. The obtained samples were placed in HCl solution for 24 h, and then washed with water to remove the acid, and finally dried at 80 °C [89].

3.3. Hot-Wire Annealing Method

In addition to the high temperature hydrogenation reduction and solid-phase reduction, researchers have also explored some other methods to synthesize black TiO₂, which has made the method of preparing black TiO₂ diversified. Wang et al. proposed a simple and direct hot-wire annealing (HWA) method [73]. The titanium dioxide nanorods were treated with highly active atomic hydrogen simply generated by hot wire [73]. The reduction mechanism was similar to that of the high temperature hydrogenation [73]. The resulted black TiO₂ nanorods had better stability and higher photocurrent density compared with the traditional hydrogenation method [73]. In addition, it had no damage to the photoelectric chemical devices [73].

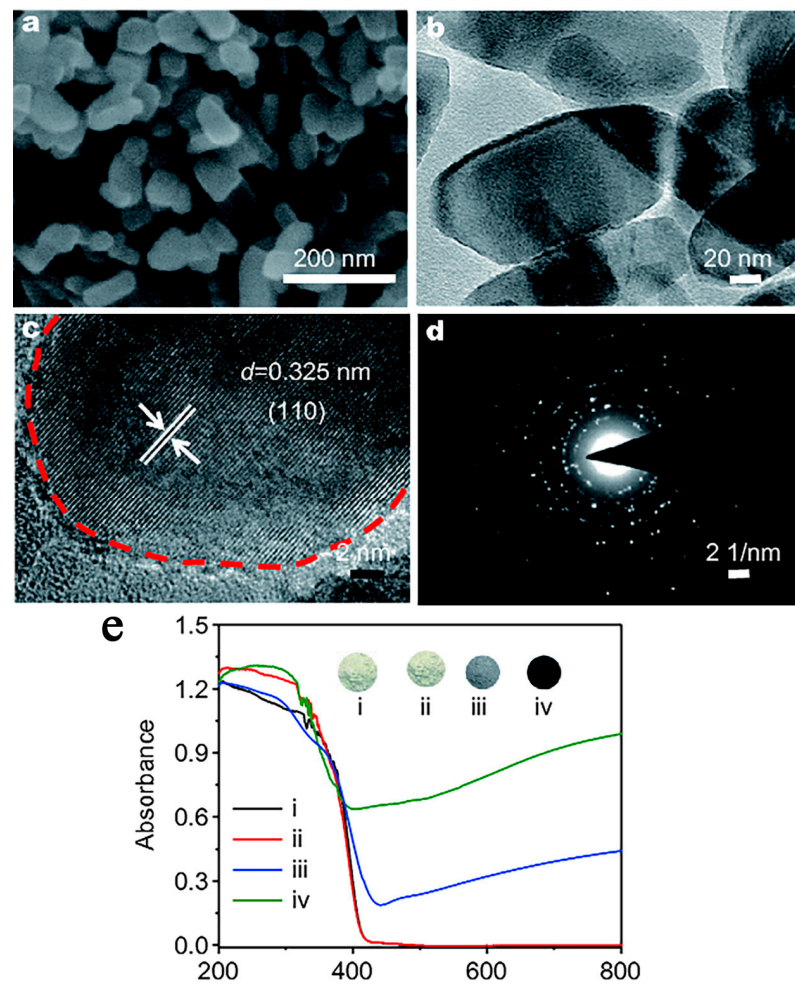


Figure 6. SEM (a), TEM (b), HRTEM images (c), the corresponding selected-area electron diffraction pattern (d) of the hydrogenated rutile TiO_2 (300 °C) and the UV/vis absorption spectra (e) of the pristine rutile TiO_2 (i) and the hydrogenated rutile TiO_2 under 250 °C (ii), 300 °C (iii), and 350 °C (iv). Reprinted with permission for ref. [87]. Copyright 2018, Springer.

3.4. Anode Oxidation Method

The introduction of crystal defects to titanium dioxide can effectively extend the light absorption range to the visible light region without side effects. Anode oxidation is a simple and efficient method to synthesize defective black TiO_2 . Dong et al. successfully prepared black TiO_2 using a two-step anode oxidation method [76]. The first step was to anodize Ti foil in the ethylene glycol solution with a certain proportion of NH_4F and distilled water, and the corresponding voltage was set at 60 V [76]. After 10 h of oxidation, an oxide layer was obtained [76]. Subsequently, the Ti foil was purified to remove organic impurities, and treated at high temperature (450 °C) for 1 h to form black TiO_2 [76].

3.5. Plasma Treatment

Zhu et al. prepared black TiO_2 nanoparticles via the one-step solution plasma method under mild conditions [27]. The structural disorder layer was assumed to be formed in TiO_2 after the solution plasma process [27]. The light absorption of TiO_2 in the visible and near infrared range was significantly enhanced after the plasma treatment, thus increasing its activity in the water evaporation under solar illumination [27]. Teng et al. prepared black TiO_2 using P25 as the precursor system, hydrogen plasma, and a hot filament chemical vapor deposition (HFCVD) device with H_2 as the reducing gas [77]. The visible and near-infrared light absorption of TiO_2 were much enhanced after the surface reduction [77]. Oxygen

vacancies and Ti-H bonds were formed on the black TiO₂ surface, thereby improving the photocatalytic activity [77].

3.6. Gel Combustion

Ullattil et al. prepared black anatase TiO_{2-x} photocatalysts through a one-pot gel combustion process using titanium butoxide, diethylene glycol, and water as precursors [90]. Plenty of Ti³⁺ and oxygen vacancies existed in the synthesized black anatase TiO₂ nanocrystals confirmed by XPS measurements [90]. The light absorption of TiO₂ was extended from UV to the near-infrared range [90]. Campbell et al. also synthesized black TiO₂ via the sol-gel combustion method using titanium tetraisopropoxide as the precursor [91]. The light absorption ability was significantly enhanced compared to commercial TiO₂ [91]. The obtained black TiO₂ with the high surface area demonstrated much improved photocatalytic degradation efficiency of the organic dye under the visible light irradiation [91].

4. Strategies for Promoting Photocatalytic Activity of Black TiO₂

Researchers have been trying to use metal and non-metal doping methods to prepare the modified TiO₂ with better light absorption ability and photocatalytic activity. The introduction of metal ions and non-metallic elements into the TiO₂ lattice can expand its absorption range to the visible light, thus enhancing the photocatalytic performance [92]. In recent years, doped black TiO₂ has also been widely explored to narrow its band gap, thereby improving its optical properties in the visible light region, and enhancing its photocatalytic activity in various reactions.

4.1. Metallic Doped Black TiO₂

It was found that by doping different metals in TiO₂, Ti⁴⁺ in TiO₂ lattice was replaced [93]. New impurity levels would be introduced in the band gap of TiO₂ [93]. The band gap would be narrowed by the doping process, thus improving the separation efficiency of the photoelectron-hole of TiO₂, increasing the quantum yield, and expanding the light absorption to the visible light region [92]. Photocatalytic degradation, hydrogen production capacity, and light energy conversion can be significantly improved [92]. Previously, various metal elements, including Cu, Co, Mn, Fe, Mo, etc., had been used to produce the doped TiO₂ via different approaches [93]. Lately, some of the metal elements, such as Al, Ni, Na, etc., were also utilized to dope black TiO₂ for achieving the narrower band gap and better photocatalytic performance [47,94,95].

Yi et al. prepared the amorphous Al-Ti-O nanostructure in black TiO₂ via a scalable and low-cost strategy [94]. The commercial TiO₂ and Al powders were mixed and then grinded in an agate mortar at room temperature for 0-50 min [94]. The color of the light gray TiO₂ turned into gray after 2 min of milling [94]. Its color became much darker after the longer milling time [94]. Black Al-Ti-O oxide samples were obtained after milling for more than 5 min [94]. The color changes, UV-Vis-NIR diffuse reflectance spectra, and TEM image of the samples were shown in Figure 7 [94]. The crystalline Al and anatase TiO₂ were transformed into amorphous Al-black TiO₂ after the ball milling [94]. Al-black TiO₂ after 20 min milling exhibited the best light absorption in the visible light and near infrared region [94].

Zhang et al. prepared Ni²⁺-doped porous black TiO₂ photocatalysts through the combination of the sol-gel method and in situ solid-state chemical reduction process [95]. The reduction approach was performed by heating the mixture of Ni-doped TiO₂ and NaBH₄ at 350 °C under Ar atmosphere for 1 h [95]. The color of the white as-made TiO₂ became yellowish after Ni doping [95]. Black Ni-doped TiO₂ was obtained after the reduction with NaBH₄ [95]. Figure 8 shows the optical properties and the band gap of different materials [95]. The light absorption of TiO₂ was extended to the visible light range after Ni doping, and further enhanced after the chemical reduction, which was attributed to the generation of oxygen vacancies, Ti³⁺, and Ni²⁺ [95]. The band gap of the black Ni-doped TiO₂ was only 1.96 eV [95].

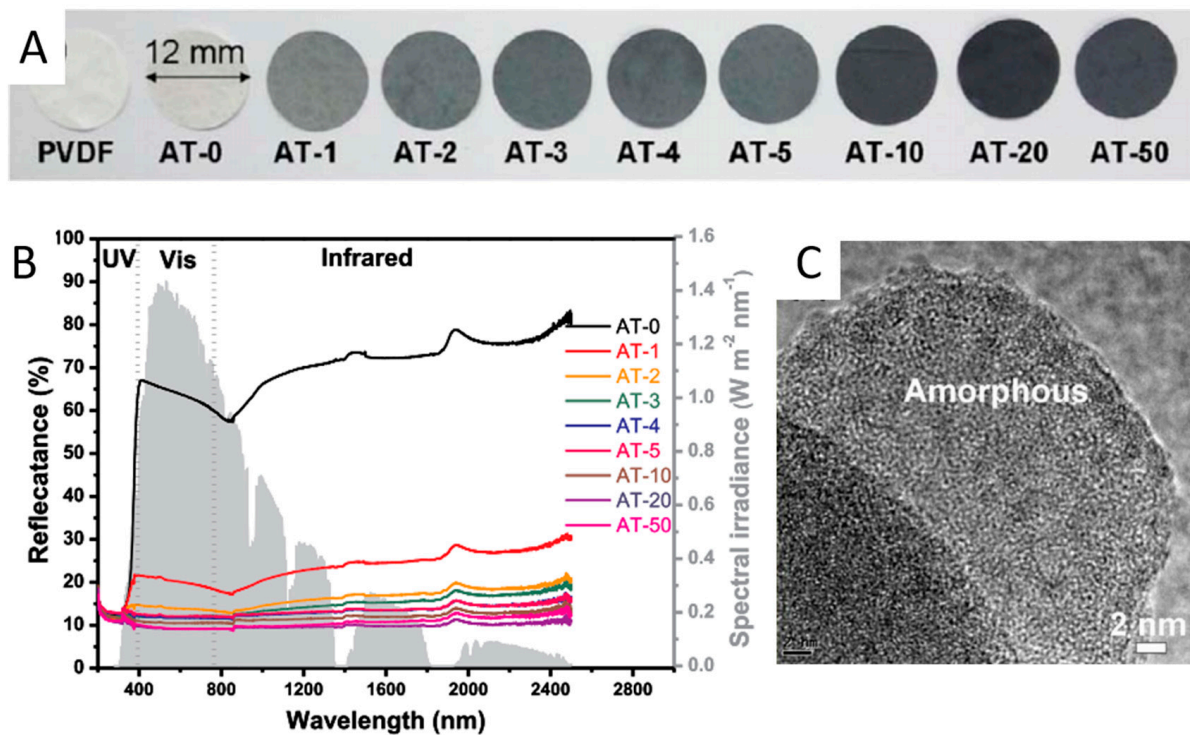


Figure 7. (A) the set of the AT-x (Al-Ti-O-milling time) membranes; (B) UV-Vis-NIR diffuse reflectance spectra of AT-x; (C) TEM image of Al-black TiO₂. Reprinted with permission for ref. [94]. Copyright 2017, Elsevier.

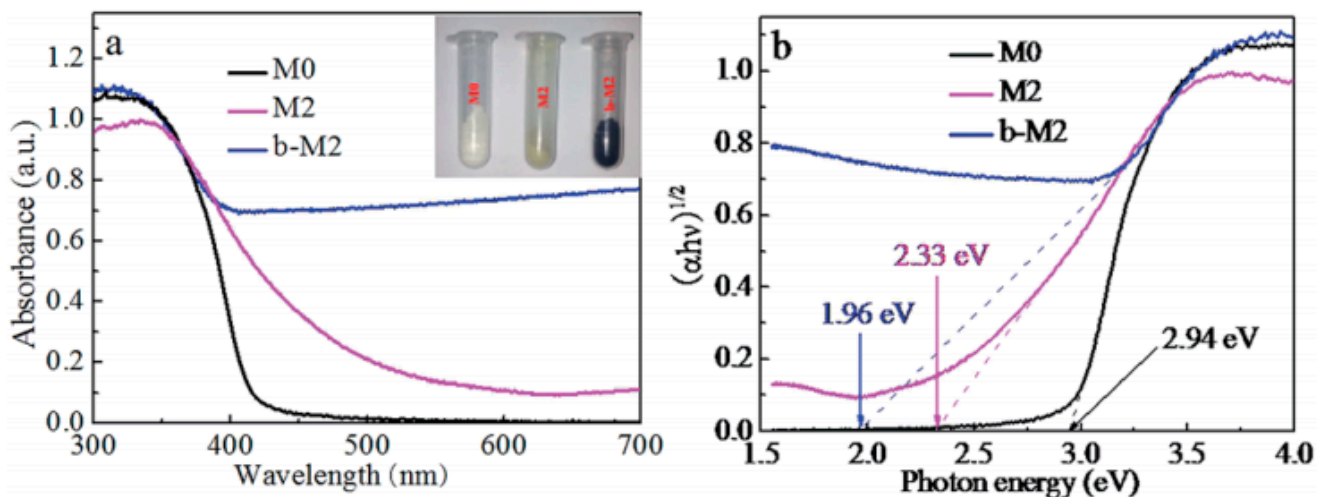


Figure 8. (a) UV-vis absorption spectra of TiO₂ (M0), Ni-doped TiO₂ (M2), and black Ni-TiO₂ (b-M2); (b) band gap for M0, M2, and b-M2 samples, respectively. Reprinted with permission for ref. [95]. Copyright 2015, The Royal Society of Chemistry.

Zhang et al. reported Ti³⁺ self-doped black TiO₂ nanotubes with mesoporous nanosheet structure via a two-step approach consisting of the solvothermal reaction and hydrogenation process [82]. The appearance of the white TiO₂ turned into black after hydrogenation at 600 °C for 2 h [82]. The optical absorption was significantly extended to the range of 400–800 nm after hydrogenation [82]. The band gap of pristine TiO₂ decreased from 3.2 eV to 2.87 eV after the surface hydrogenation [82].

4.2. Non-Metallic Doped Black TiO₂

The doping mechanism of nonmetallic elements can be explained as follows: the doped elements act as overlapping impurity levels in the valence band inside the photocatalyst crystal, thereby reducing the band gap of semiconductors and promoting the migration of photogenerated electrons to the active site. The doping of non-metal elements in the crystal lattice of TiO₂ can slow down the electron-hole pair recombination rate, which is an effective modification way to improve the photocatalytic activity of TiO₂.

The nitrogen atom, which has five outer shell electrons, has a similar radius to oxygen. The introduction of N into TiO₂ enhances its visible light photocatalytic activity, which is proved to be the most ideal non-metallic doping element in a large number of studies [96,97]. Since the 2p orbital of N has a similar energy level to that of the oxygen atom and is easy to hybridize, the researchers found that the doping of N can improve the defects of TiO₂ and broaden the response range of the absorption spectra [98]. The N-Ti-O bond generated by doping the crystal can change the energy level structure of TiO₂ and improve the quantum efficiency [99]. In addition, N can also replace O in the lattice with the formation of the Ti-N bond, which increases the absorption of the visible light by TiO₂ and improves the photocatalytic efficiency of TiO₂ [96].

Zhou et al. successfully synthesized the nitrogen-doped black titanium dioxide nanocatalyst by calcining white TiO₂ with or without urea at varied temperatures under the different atmosphere [31]. The N-doped TiO₂ using urea as N precursor has a better visible light absorption, narrower band gap and the most effective excitation charge separation, and higher photocatalytic activity [31]. Liu et al. prepared N-doped black TiO₂ spheres via a two-step process consisting of the solvothermal reaction and calcination in the nitrogen atmosphere [100]. The black N-TiO₂ photocatalysts were obtained after heat treatment at 500 °C in N₂ atmosphere for 3 h [100]. Ammonium chloride was used as the nitrogen source during the synthetic process [100]. The obtained black N-TiO₂ with a moderate mole ratio of ammonium chloride to TiO₂ (2:1) had the narrowest band gap and the highest photocatalytic pollutant degradation efficiency [100].

Gao et al. prepared black TiO₂ nanotube arrays with dual defects consisting of bulk N doping and surface oxygen vacancies [101]. Urea was utilized as the N precursor during the anodic oxidation process [101]. Black N-doped TiO₂ nanotube arrays were obtained after calcination at 600 °C in the Ar atmosphere using aluminum powder [101]. The doping of N generated a new energy level and shortened the carrier migration distance [101]. The synergistic effect of the two defects established an internal electric field, promoted the transfer of charge, and achieved the balance between kinetics and thermodynamics, thereby enhancing the photocatalytic hydrogen production efficiency [101].

Cao et al. successfully synthesized N and Ti³⁺ co-doped mesoporous black TiO₂ hollow spheres (N-TiO_{2-x}) by a step-by-step method [102]. The prepared three different kinds of TiO₂ had similar XRD peaks, indicating no impurities was formed during the synthetic process, as presented in Figure 9a [102]. The broader peaks of the black TiO₂ may be attributed to the lattice distortion caused by N doping [102]. Raman spectra (Figure 9b) showed that the main phase of the titanium dioxide hollow sphere was anatase [102]. The co-doping of Ti³⁺ and N in N-TiO_{2-x} resulted in a certain amount of attenuation [102]. The absorption in the visible light was much enhanced after the co-doping of N and Ti³⁺ in TiO₂ [102]. The color of the samples gradually became darker after the nitrogen and Ti³⁺ doping [102]. In addition, the band gap of the black N-doped TiO₂ was much smaller than the pristine TiO₂ (Figure 9c,d) [102]. The charge separation and photocatalytic activity for photocatalytic pollutant removal and hydrogen generation were much improved after the co-doping of N and Ti³⁺ in the lattice of TiO₂ (Figure 9e) [102].

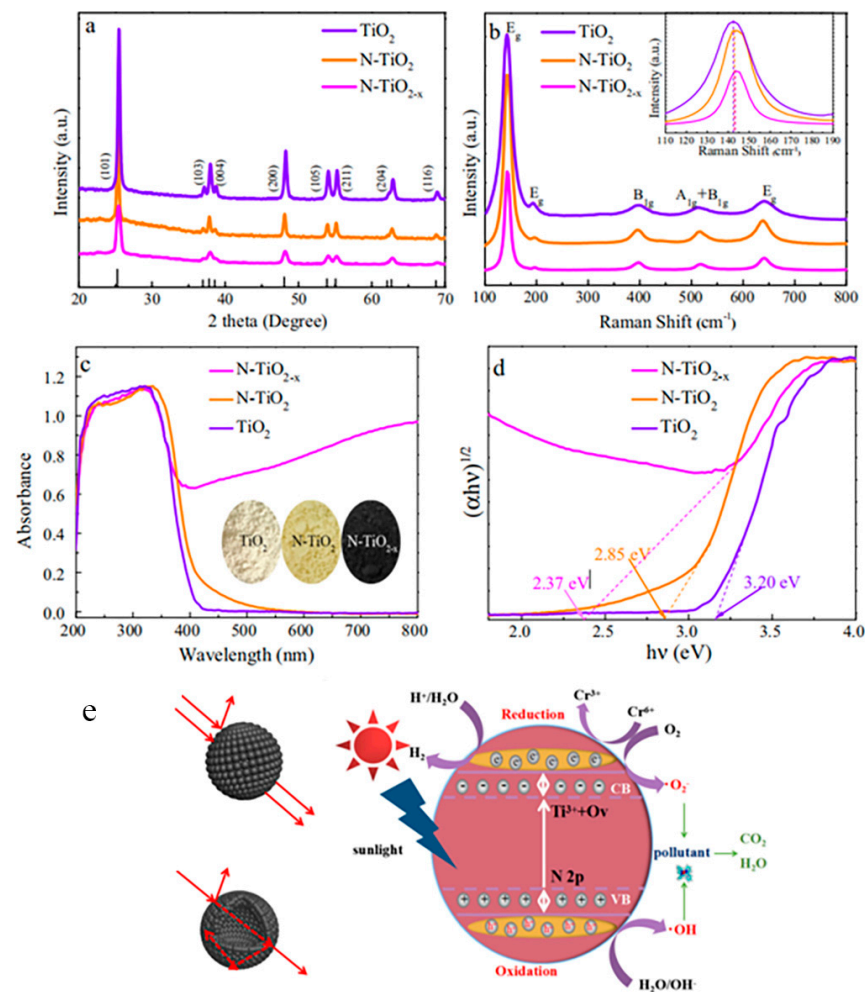


Figure 9. XRD patterns (a), Raman spectra (b), UV-vis adsorption spectra (c), and determination of the indirect interband transition energies (d) of TiO_2 , N-TiO_2 , and N-TiO_{2-x} , respectively. Schematic diagrams of light pathways in nanoparticles, hollow spheres, and schematic illustration for the solar-driven photocatalytic mechanism of N-TiO_{2-x} (e). Reprinted with permission for ref. [102]. Copyright 2017, Elsevier.

4.3. Metal-Loaded Black TiO_2

Metal nanoparticles, such as Ag, Cu, Pt, etc., can generate the surface plasmon resonance (SPR) effect, thus improving the UV-vis absorption ability of photocatalysts [103]. The introduction of metal nanoparticles or clusters to the black TiO_2 photocatalyst surface could further expand its light absorption range and enhance the photo-induced charge separation and transfer efficiency, thus improving the photocatalytic performance [38,104–109]. Silver nanoparticles or clusters have been extensively explored to construct Ag/black TiO_2 photocatalysts due to the relatively lower cost of Ag than other noble metals and the SPR effect. Jiang et al. prepared the Ag-decorated 3D urchinlike N-TiO_{2-x} via a facile photo-deposition method combined with a reduction process, as presented in Figure 10 [104]. The AgNO_3 solution was used as the Ag precursor and deposited onto the N-TiO_2 surface under UV illumination at the wavelength of 365 nm for 30 min [104]. Notably, the unique 3D urchinlike structure was retained after the Ag deposition and NaBH_4 reduction process [104]. The light absorption of photocatalysts in the visible light range was further enhanced after the Ag deposition, with a much smaller band gap (2.61 eV) [104]. The Ag/ N-TiO_{2-x} photocatalysts presented the most excellent photocatalytic H_2 production rate ($186.2 \mu\text{mol h}^{-1} \text{g}^{-1}$) [104].

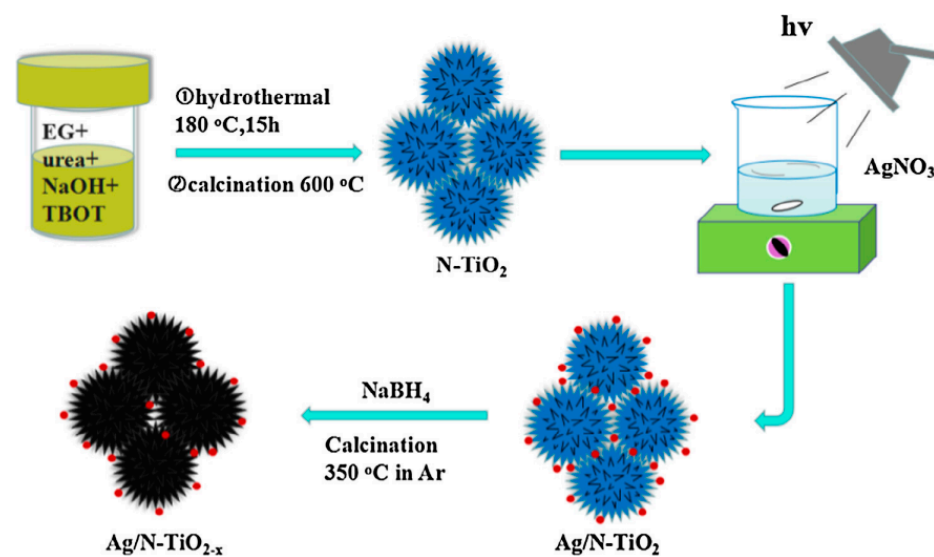


Figure 10. Schematic illustration for preparation of 3D urchinlike Ag/N-TiO_{2-x}. Reprinted with permission for ref. [104]. Copyright 2018, Elsevier.

Li et al. constructed Ag nanoparticle-decorated black TiO₂ foams through the wet impregnation and high temperature surface hydrogenation process [105]. Ag nanoparticles were formed in the open pores of black TiO₂ foams after the hydrogen atmosphere reduction, thus decreasing its surface area [105]. The synthetic process and UV-vis absorption spectra of Ag-black TiO₂ foams were presented in Figure 11 [105]. The Ag-black TiO₂ foams with varied amounts of silver showed apparent absorption at around 500 nm thanks to the SPR effect of Ag nanoparticles [105]. The Ag-black TiO₂ foams containing 3 wt.% Ag nanoparticles exhibit the highest photocatalytic efficiency for atrazine removal [105]. Excess amounts of Ag nanoparticles in black TiO₂ foams would decrease its photocatalytic performance due to the aggregation of Ag nanoparticles [105]. Ag nanoparticles were also decorated onto black TiO₂ nanorods [106,109] and nanotubes surface [38], to further improve its photocatalytic performance using the SPR effect. In addition, NiS and Pt nanoparticles were co-decorated onto the surface of black TiO₂ nanotubes via the solvothermal and photo-deposition approach, respectively [109]. The SPR effect of Pt nanoparticles effectively improved the light absorption ability, thus enhancing the photocatalytic water splitting [109]. Wang et al. successfully deposited Pt single atoms onto the black TiO_{2-x}/Cu_xO surface assisted by the presence of surface oxygen vacancies [110]. The deposition of Pt single atoms further improved the light absorption of black TiO_{2-x}/Cu_xO in the entire visible region [110]. Cu, which was a much cheaper candidate than noble metal, was also used for the surface decoration of black TiO₂ surface as a SPR effect metal, thereby improving its photothermal effect [108].

4.4. Construction of Black TiO₂ Based Heterojunction Photocatalysts

Although the visible light absorption ability of TiO₂ has been much enhanced after the hydrogenation or reduction process, the charge separation and transfer efficiency of black TiO₂ is still far from satisfactory for photocatalytic applications. In addition to the surface modification with metal nanoparticles, the construction of black TiO₂-based junctions is an efficient way to improve the photo-generated charge separation and migration efficiency. The types of black TiO₂-based heterojunctions can be divided into three main categories, including type II heterojunctions [59,111–119], Z-scheme heterojunctions [120], and tandem heterojunctions [29,121,122]. Tan et al. fabricated the Ti³⁺-TiO₂/g-C₃N₄ nanosheets heterojunctions through a facile calcinations-sonication assisted approach [118]. The photo absorption of Ti³⁺-TiO₂ in the visible light range had been evidently enhanced after the coupling with meso-g-C₃N₄ [118]. The synthetic procedure of Ti³⁺-TiO₂/g-C₃N₄ nanosheets, the UV-vis absorption spectra, and the band gaps of different samples were shown in

Figure 12 [118]. The separation and migration of the photo-induced charge carrier had been effectively improved due to the construction of heterojunctions [118]. Ti^{3+} - TiO_2 / $\text{g-C}_3\text{N}_4$ nanosheets exhibited the highest photocatalytic H_2 evolution rate and phenol degradation efficiency [118]. A type II heterojunction with enhanced charge separation and transfer efficiency had been proposed [118].

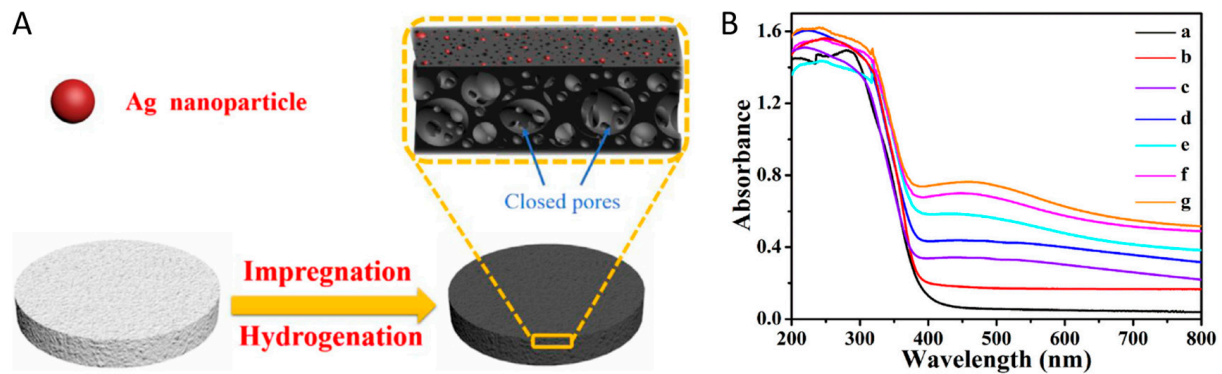


Figure 11. (A) Schematic view for the synthetic process of Ag/black TiO_2 foams; (B) The UV-vis absorption spectra of black TiO_2 foams (a) and Ag-black TiO_2 foams with different Ag contents of 0.5 (b), 1 (c), 2 (d), 3 (e), 4 (f), and 5 wt.% (g). Reprinted with permission for ref. [105]. Copyright 2018, Elsevier.

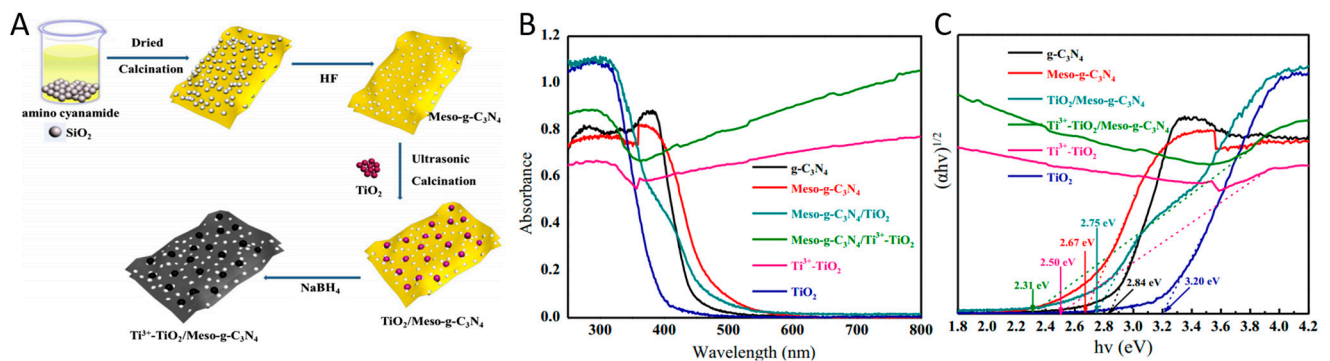


Figure 12. (A) The synthetic process of Ti^{3+} - TiO_2 / $\text{g-C}_3\text{N}_4$ nanosheets heterojunctions; (B) UV-vis diffuse reflectance spectra; (C) the corresponding calculated band gaps. Reprinted with permission for ref. [118]. Copyright 2018, Elsevier.

Ren et al. prepared magnetic $\gamma\text{-Fe}_2\text{O}_3$ /black TiO_2 heterojunctions via the metal-ion intervened hydrothermal method and high temperature hydrogenation process [59]. In addition, $\alpha\text{-Fe}_2\text{O}_3$ nanosheets were transformed to the surface defected $\gamma\text{-Fe}_2\text{O}_3$ after the hydrogenation process [59]. The light utilization of black TiO_2 in visible light even near the infrared region has been improved after the combination with $\gamma\text{-Fe}_2\text{O}_3$ [59]. Figure 13 presented the UV-vis absorption spectra and the proposed band structure and charge transfer mechanism of $\gamma\text{-Fe}_2\text{O}_3$ /black TiO_2 heterojunctions [59]. The fabrication of the type II heterojunctions efficiently enhanced the photo-generated charge separation and transfer process [59]. The photocatalytic degradation of tetracycline on the heterojunction photocatalysts surface had been much improved, compared with the pristine TiO_2 [59]. In addition, Bi_2MoO_6 [111], CdS [115], CeO_2 [117], SrTiO_3 [119], etc. had also been used for the construction of type II heterojunctions with black TiO_2 with much improved photocatalytic efficiency.

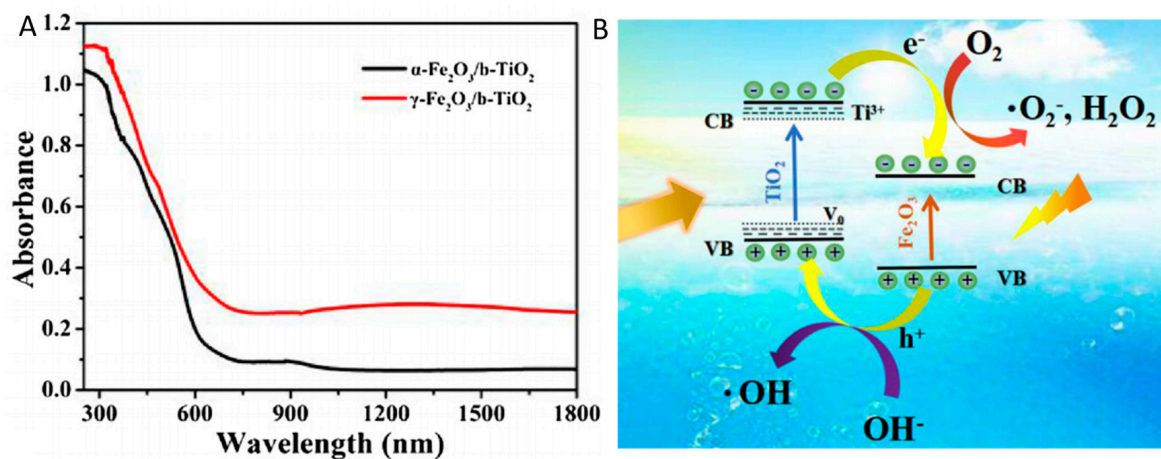


Figure 13. (A) UV-vis spectra; (B) Proposed band alignment and charge transfer mechanism. Reprinted with permission for ref. [59]. Copyright 2019, Elsevier.

Sun et al. synthesized the CdS quantum dots/defective $\text{ZnO}_{1-x}\text{-TiO}_{2-x}$ Z scheme heterojunction via the combination of hydrothermal synthesis, chemical reduction, and electroless plating process [120]. The visible light absorption was enhanced by the formation of ZnO-TiO_2 heterojunction, and further improved after combining with CdS [120]. The formation process of the heterojunction, UV-vis spectra, and proposed charge transfer mechanism are shown in Figure 14 [120]. The charge separation efficiency and photocatalytic organic pollutant removal rate were much improved upon the formation of CdS QDs/defective $\text{ZnO}_{1-x}\text{-TiO}_{2-x}$ Z scheme heterojunction [120].

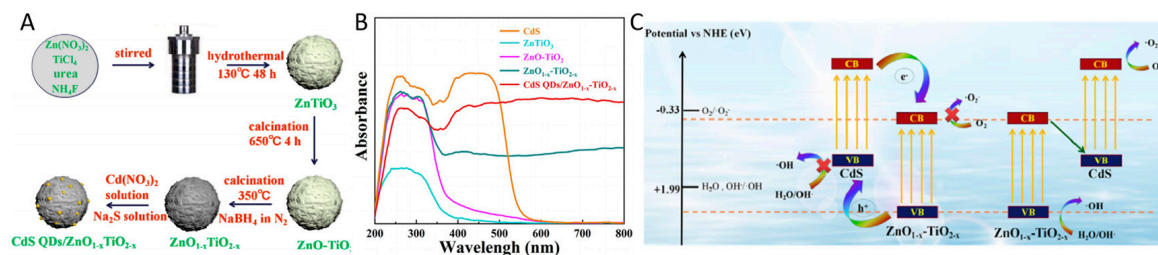


Figure 14. (A) Formation process of CdS QDs/ $\text{ZnO}_{1-x}\text{-TiO}_{2-x}$; (B) UV-vis spectra; (C) Proposed band alignment and charge transfer mechanism. Reprinted with permission for ref. [120]. Copyright 2020, Elsevier.

To further promote the visible light utilization and photo-induced charge separation and transfer efficiency, black TiO_2 -based tandem heterojunction photocatalysts have been proposed by researchers for photocatalytic hydrogen production. Sun et al. prepared a hierarchical hollow black $\text{TiO}_2/\text{MoS}_2/\text{CdS}$ tandem heterojunction photocatalyst through the combination of the solvothermal method and high-temperature hydrogenation treatment [122]. The black $\text{TiO}_2/\text{MoS}_2$ heterojunction effectively enhanced the photon absorption in visible light and the near infrared region [122]. The tandem system further promoted visible light utilization compared to other combinations [122]. The schematic view of the construction of black $\text{TiO}_2/\text{MoS}_2/\text{CdS}$, UV-vis absorption spectra, and photocatalytic hydrogen evolution rate are illustrated in Figure 15. The charge separation and migration efficiency were much promoted by the formation of black $\text{TiO}_2/\text{MoS}_2/\text{CdS}$ tandem heterojunction [122]. The tandem heterojunction exhibited the highest photocatalytic hydrogen production rate under AM 1.5 illumination [122]. In addition, a sandwich-like mesoporous black $\text{TiO}_2/\text{MoS}_2/\text{black TiO}_2$ nanosheet photocatalyst was proposed for visible light photocatalytic hydrogen generation with a much-promoted photo-generated charge transfer efficiency [121]. The mesoporous TiO_2 and Cu_2S were also combined with MoS_2 to synthesize the hierarchical tandem heterojunctions [29]. The near-infrared energy

utilization was enhanced by the tandem system, thereby promoting the photothermal effect [29]. The visible light photocatalytic H₂ generation rate was significantly improved, achieving 3376.7 $\mu\text{mol h}^{-1} \text{g}^{-1}$, which was approximately 16 times that of black TiO₂ [29].

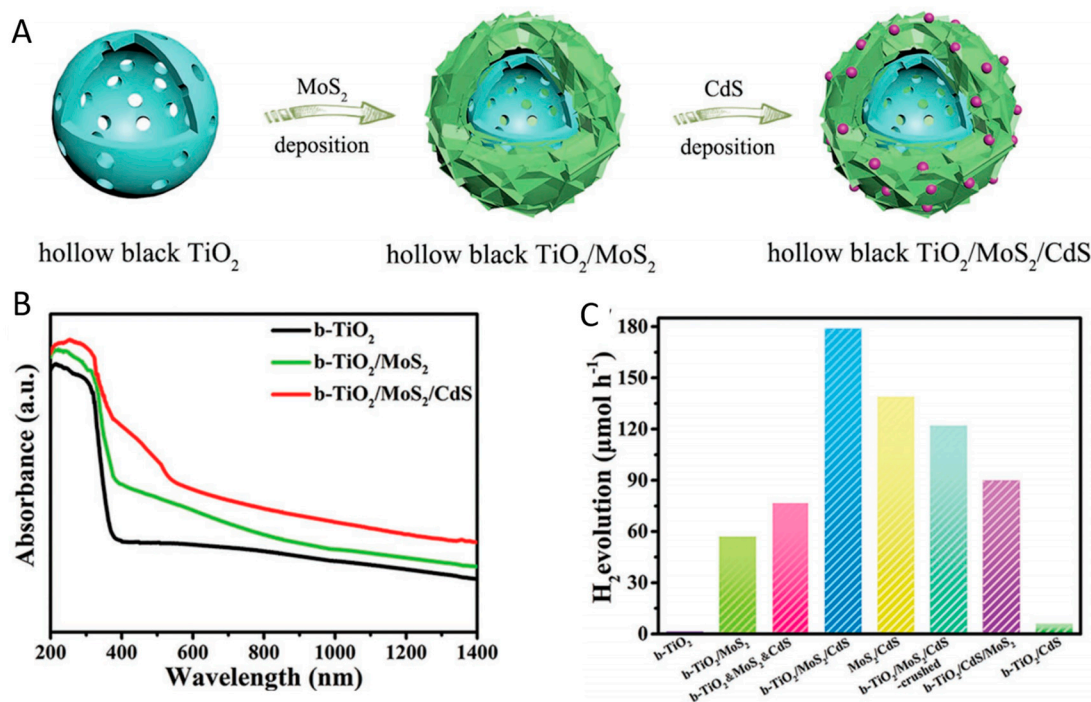


Figure 15. (A) Schematic illustration for the formation of TiO₂/MoS₂/CdS, (B) UV-vis spectra, (C) photocatalytic H₂ evolution measurements. Reprinted with permission for ref. [122]. Copyright 2018, Wiley-VCH.

5. Applications of Black TiO₂

The absorption of light can be extended from the ultraviolet light to visible light, and even to near-infrared light by changing the white TiO₂ into black TiO₂ via various methods. This strategy can be utilized for enhancing the photocatalytic activity in the visible light range. Changing the color of TiO₂ from white to black is one of most efficient ways for improving its photocatalytic efficiency in various fields, such as photocatalytic water splitting, photocatalytic pollutant degradation, etc.

5.1. Photocatalytic Water Splitting

Black TiO₂ has a modified band structure, thereby improving the charge separation and migration efficiency. Its enhanced photocatalytic performance has been extensively investigated in water splitting. Black mesoporous TiO₂ synthesized by Zhou et al. has excellent hydrogen production performance [79]. As shown in Figure 16A, black TiO₂ had a higher rate of hydrogen production than original TiO₂ under the condition of AM 1.5G and had excellent hydrogen production ability in visible light [79]. In addition, almost no attenuation was detected during photocatalytic measurements after 10 cycles [79]. As presented in Figure 16B, its apparent quantum efficiency at each single wavelength was much higher than that of the original sample [79]. The mesoporous black TiO₂ photocatalysts showed remarkable photocatalytic stability in 10 cycling hydrogen evolution measurements within 30 h (each cycling test was conducted in the presence of fresh 1 mL methanol) [79]. The black TiO₂ nanotubes prepared by Yang et al. showed an excellent photocatalytic hydrogen production performance (9.8 $\text{mmol h}^{-1} \text{g}^{-1}$) through high temperature hydrogenation [80]. The enhanced photocatalytic activity could be attributed to two aspects: (1) the special one-dimensional hollow tube structure improved the charge separation efficiency; (2) the high temperature hydrogenation strategy improved its ability for sunlight utilization [80]. The

photocatalytic activity of the black TiO₂ nanotubes for H₂ production remained stable for 5 cycles in 15 h using H₂PtCl₆ as the co-catalyst and methanol as the sacrificing agent [80].

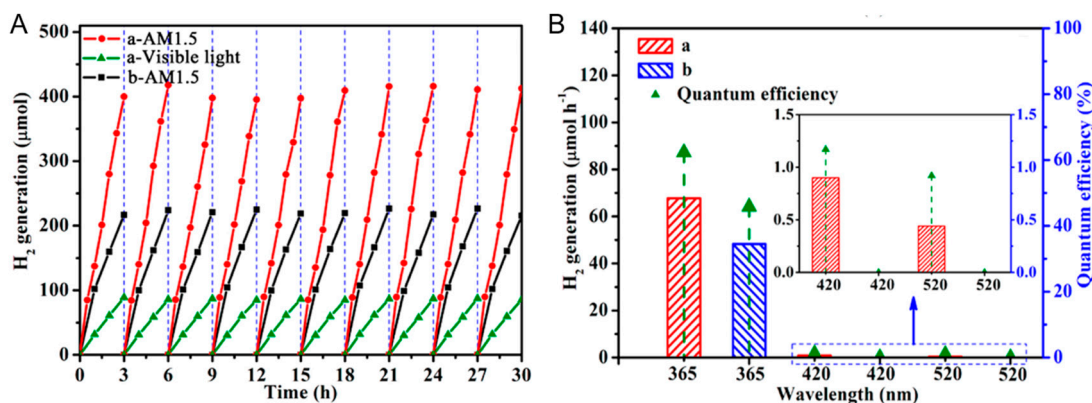


Figure 16. Photocatalytic hydrogen evolution of the ordered mesoporous black TiO₂ (a) and pristine ordered mesoporous TiO₂ materials (b). (A) Cycling tests of photocatalytic hydrogen generation under AM 1.5 and visible light irradiation. (B) The photocatalytic hydrogen evolution rates under single-wavelength light and the corresponding QE. The inset enlarges the QE of single-wavelength light at 420 and 520 nm. Reprinted with permission for ref. [79]. Copyright 2014, American Chemical Society.

Two-dimensional lamellar structures with plenty of active sites are often used in TiO₂ photocatalysis because of their large specific surface area. The black TiO₂ nanosheets prepared by Zhang et al. shortened the band gap to 2.85 eV, thereby broadening the light response to the visible light region [123]. The hydrogen production rate was up to 165 μmol h⁻¹ 0.05 g⁻¹, which was twice as much as that of the original sample [123]. The chemical stability, light corrosion resistance, and photocatalytic activity for H₂ generation were confirmed by 5 cycling tests in 25 h, using H₂PtCl₆ and methanol as the co-catalyst and sacrificing agent, respectively [123]. Similarly, Wu et al. synthesized another black TiO₂ nanosheets, which had a high hydrogen production rate of 3.73 mmol h⁻¹ g⁻¹ [83]. This photocatalyst exhibited an unchanged photocatalytic H₂ evolution rate in 5 cycling measurements with 15 h [83]. Li et al. designed and synthesized black TiO₂ nanospheres by the self-assembly solvothermal method combined with the hydrogenation strategy [81]. The charge separation efficiency had been effectively improved after the hydrogenation process, confirmed by experimental results and DFT calculations [81]. The photocatalytic performance for H₂ formation was also repeated 5 times in 15 h and remained stable in the 5 cycles [81].

The black rutile TiO₂ prepared by Xiao et al. by the solid-phase reduction method showed much-enhanced hydrogen production performance, stability, and high apparent quantum efficiency, which was about 1.5 times that of the original sample (Figure 17) [87]. In addition, the defects in TiO₂ could be regulated by varying the hydrogenation temperature, and the optimal hydrogenation temperature was proved to be 300 °C [87]. The stability of photocatalytic activity was verified by 5 cycling hydrogen formation measurements in 12 h under AM 1.5 illumination [87]. No obvious decrease in the activity was observed in the cycling tests [87]. The maximum hydrogen production rate of black TiO₂ synthesized by Sinhamahapatra et al. using the controllable magnesium thermal reduction method was 43 mmol h⁻¹ g⁻¹ in the full solar wavelength range with excellent stability, which was better than the black TiO₂ material previously reported [89]. The black TiO₂ nanoparticles presented great stability in the photocatalytic hydrogen evolution confirmed by 10 cycling measurements, which were conducted for 10 consecutive days using the same solution [89]. The aging of the black TiO₂ materials was generally not mentioned in the reported publications. The photocatalytic stability of the hydrogen generation was mostly measured in 5 cycling tests within 15 h using the same solution. Some photocatalysts were

tested in 10 repeated photocatalytic hydrogen formation measurements for more than 20 h. Black TiO₂ photocatalysts usually showed good stability and light corrosion resistance in the photocatalytic H₂ evolution reaction, providing the possibility of long-term usage of black TiO₂ photocatalysts for H₂ production.

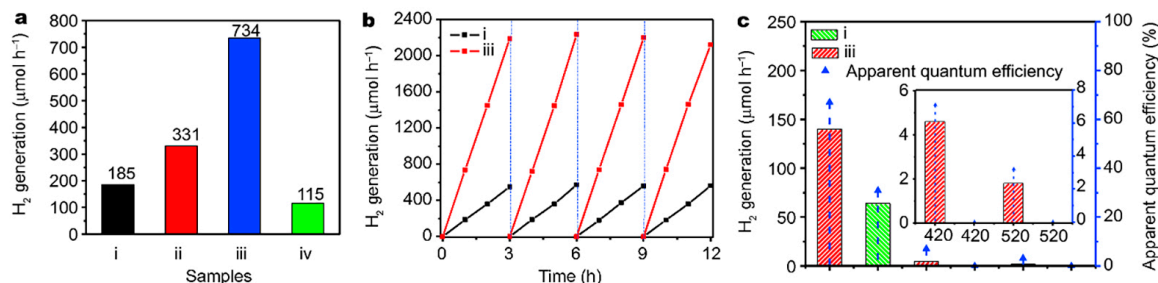


Figure 17. (a) Photocatalytic hydrogen evolution rates, (b) cycling tests of photocatalytic hydrogen generation under AM 1.5 irradiation, (c) the single wavelength photocatalytic hydrogen evolution rates of pristine TiO₂ (i), and hydrogenated TiO₂ at 250 °C (ii), 300 °C (iii), and 350 °C (iv), respectively. Reprinted with permission for ref. [87]. Copyright 2018, Springer.

5.2. Photocatalytic Degradation of Pollutants

In addition to the hydrogen production, pollutant degradation is also one of the main applications of photocatalysis. Titanium dioxide was often used in the photocatalytic degradation of organic dye and pesticides [124–126]. Black TiO₂ with an enhanced light absorption ability would have much improved the photocatalytic pollutant removal efficiency. The black TiO₂ obtained by CaH₂ reduction not only presented an enhanced hydrogen generation rate, which was 1.7 times that of the original sample, but also achieved a huge improvement in the degradation of pollutants with the complete removal of methyl orange within 8 min [72]. Hamad et al. synthesized black TiO₂ using a new method of controlled hydrolysis [85]. The oxygen vacancy concentration was significantly increased with a much-reduced band gap, thereby showing an excellent organic pollutant degradation rate under visible light irradiation [85].

The oxygen vacancy plays an important role in photocatalysis. Black TiO₂ prepared by Teng et al. via vapor deposition had a high photocatalytic oxidation activity for organic pollutants in the water, due to the formation of Ti-H bonds and a large number of oxygen vacancies [77]. All pollutants (rhodamine B) could be completely degraded within 50 min detected by the UV-vis spectrophotometer [77]. The defective TiO_{2-x} prepared by the anodic oxidation method was characterized by the electron paramagnetic resonance spectroscopy, confirming the existence of oxygen vacancies and the extension of the absorption from the ultraviolet to visible light region [76]. This black TiO₂ material showed excellent photocatalytic degradation activity for rhodamine B under 400–500 nm light irradiation [76].

The black TiO₂-based heterojunction could significantly improve its photocatalytic efficiency in pollutant remediation thanks to the enhanced charge separation and transfer efficiency. Jiang et al. prepared black TiO₂/Cu₂O/Cu composites via in-situ photodeposition and the solid reduction method [127]. The light energy harvesting in the visible and infrared range was much enhanced after the formation of the composites [127]. The photocatalytic efficiency of the composites for Rhodamine B degradation was improved compared with the commercial P25, due to the enhanced charge separation efficiency [127]. Qiang et al. synthesized the RuTe₂/black TiO₂ photocatalyst through gel calcination and the microwave-assisted process [128]. The light absorption range of the as-made composites was enlarged compared to the pristine TiO₂. The photocatalytic efficiency of the diclofenac degradation was 1.2 times higher than the pure black TiO₂ [128]. The stability of RuTe₂/black TiO₂ for the photocatalytic diclofenac degradation was confirmed via 5 repeated experiments [128].

Tetracycline is a toxic antibiotic which is difficult to remove. Li et al. synthesized black TiO₂ modified with Ag/La presented an improved visible light photocatalytic performance for the tetracycline degradation [26]. The photocatalytic stability and reusability of black TiO₂-based photocatalysts were studied via 5 cycling tests without apparent deactivation [26]. Wu et al. reported that the synthesized black anatase TiO₂ exhibited impressive photocatalytic degradation of tetracycline [84]. Its degradation efficiency of tetracycline was 66.2% under the visible light illumination, which was higher than that of the white titanium dioxide and doped titanium dioxide [84]. In addition, ·O²⁻ and h⁺ were found to play important roles in the degradation process, which was different from the original TiO₂, providing new insights for environmental protection [84]. The stability of the photocatalytic tetracycline degradation was measured in four repeated experiments within 960 min without apparent deactivation after four cycles [84]. Table 2 summarizes the applications and photocatalytic stability of the black TiO₂ nanomaterials. The long-term photocatalytic stability of pollutant removal is often overlooked and unverified in most reported research. Therefore, researchers should pay more attention to aging and photocatalytic stability in pollutant degradation in the future.

Table 2. Applications and properties of black TiO₂ nanomaterials.

Black TiO ₂	Reducing Agent	Oxygen Vacancy	Application	Numbers of Cycling Tests	Ref.
Anatase with minor rutile	NaBH ₄	✓	Tetracycline degradation	5	[26]
Anatase and rutile	H ₂	✓	Rhodamine B degradation	N/S	[77]
Anatase	H ₂	✓	H ₂ evolution	10	[79]
Anatase	H ₂	✓	H ₂ evolution	5	[80]
Anatase	H ₂	✓	H ₂ evolution	5	[81]
Anatase	H ₂	✓	H ₂ evolution	5	[83]
Anatase	H ₂	✓	Tetracycline degradation	4	[84]
Anatase	H ₂	N/S	Orange G degradation	N/S	[85]
Rutile	NaBH ₄	✓	H ₂ evolution	4	[87]
Anatase with minor rutile	H ₂	✓	H ₂ evolution	10	[89]
Anatase	Anodization	✓	Rhodamine B degradation	N/S	[76]
Anatase	H ₂	N/S	H ₂ evolution	5	[123]
Anatase and rutile	NaBH ₄	✓	Rhodamine B degradation	4	[127]
Anatase	H ₂	✓	Diclofenac degradation	5	[128]

Notes: N/S: not studied; ✓: yes.

6. Summary and Outlooks

The utilization and conversion of sunlight in a more efficient way has gained much interest due to the energy crisis and global warming effect. The construction of black TiO₂-based materials is proved to be an effective approach for promoting visible light utilization. Black TiO₂ with various morphologies, such as nanospheres, nanotubes, nanowires, etc., have been rationally designed. The properties of black TiO₂, such as the surface area, are easily affected by its morphology. Although the photon absorption of TiO₂ in the visible light region can be effectively increased after the surface reduction process, its photocatalytic performance still needs to be improved for practical applications. The photocatalytic activity of black TiO₂ photocatalysts can be further enhanced by three main methods: element doping, decoration with metal nanoparticles, and fabrication of heterojunctions. The introduction of metal or nonmetal elements into the black TiO₂ lattice can create new impurities, thus narrowing its band gap. The SPR effect caused by metal decoration on the

black TiO₂ surface can efficiently improve its visible light utilization. The fabrication of black TiO₂ heterojunctions, including type II, Z scheme, and tandem heterojunctions, can significantly enhance the photo-induced charge separation and transfer efficiency, thereby promoting the photocatalytic performance. The photocatalytic activity of black TiO₂-based materials are mainly evaluated in the photocatalytic hydrogen production and pollutant removal. Although these black TiO₂-based nanomaterials exhibit excellent photocatalytic activity in the visible light region, technologies for enhancing light harvesting in near-infrared should be developed. In addition, the enhancement of the photo-generated charge separation and transfer should be further reinforced to meet the standard for practical application. Applications of black TiO₂-based materials in industrial and outdoor fields, such as self-cleaning surfaces, should also be investigated in future.

Author Contributions: Conceptualization, W.Z.; writing—original draft preparation, L.L. and M.W.; writing—review and editing, Z.L., X.W. and W.Z.; Supervision, Funding acquisition, W.Z. All authors have read and agreed to the published version of the manuscript.

Funding: We gratefully acknowledge the support of the National Natural Science Foundation of China (52172206), the Natural Science Foundation of Shandong Province (ZR2022QD062), the Special Fund for Taishan Scholars Project, and the Development Plan of Youth Innovation Team in Col-leges and Universities of Shandong Province.

Data Availability Statement: Not applicable.

Conflicts of Interest: The authors declare no conflict of interest.

References

1. Fujishima, A.; Honda, K. Electrochemical photolysis of water at a semiconductor electrode. *Nature* **1972**, *238*, 37–38. [[CrossRef](#)]
2. Xu, Y.; Kraft, M.; Xu, R. Metal-free carbonaceous electrocatalysts and photocatalysts for water splitting. *Chem. Soc. Rev.* **2016**, *45*, 3039–3052. [[CrossRef](#)] [[PubMed](#)]
3. Yao, B.; Zhang, J.; Fan, X.; He, J.; Li, Y. Surface Engineering of Nanomaterials for Photo-Electrochemical Water Splitting. *Small* **2019**, *15*, 1803746. [[CrossRef](#)]
4. Xu, S.; Carter, E.A. Theoretical Insights into Heterogeneous (Photo)electrochemical CO₂ Reduction. *Chem. Rev.* **2019**, *119*, 6631–6669. [[CrossRef](#)]
5. Zhang, B.; Sun, L. Artificial photosynthesis: Opportunities and challenges of molecular catalysts. *Chem. Soc. Rev.* **2019**, *48*, 2216–2264. [[CrossRef](#)] [[PubMed](#)]
6. Diercks, C.S.; Liu, Y.; Cordova, K.E.; Yaghi, O.M. The role of reticular chemistry in the design of CO₂ reduction catalysts. *Nat. Mater.* **2018**, *17*, 301–307. [[CrossRef](#)] [[PubMed](#)]
7. Hoffmann, M.R.; Martin, S.T.; Choi, W.; Bahnemann, D.W. Environmental Applications of Semiconductor Photocatalysis. *Chem. Rev.* **1995**, *95*, 69–96. [[CrossRef](#)]
8. Wang, H.; Zhang, L.; Chen, Z.; Hu, J.; Li, S.; Wang, Z.; Liu, J.; Wang, X. Semiconductor heterojunction photocatalysts: Design, construction, and photocatalytic performances. *Chem. Soc. Rev.* **2014**, *43*, 5234–5244. [[CrossRef](#)]
9. Calvete, M.J.F.; Piccirillo, G.; Vinagreiro, C.S.; Pereira, M.M. Hybrid materials for heterogeneous photocatalytic degradation of antibiotics. *Coord. Chem. Rev.* **2019**, *395*, 63–85. [[CrossRef](#)]
10. Schneider, J.; Matsuoka, M.; Takeuchi, M.; Zhang, J.; Horiuchi, Y.; Anpo, M.; Bahnemann, D.W. Understanding TiO₂ Photocatalysis: Mechanisms and Materials. *Chem. Rev.* **2014**, *114*, 9919–9986. [[CrossRef](#)]
11. Honda, M.; Ochiai, T.; Listiani, P.; Yamaguchi, Y.; Ichikawa, Y. Low-Temperature Synthesis of Cu-Doped Anatase TiO₂ Nanostructures via Liquid Phase Deposition Method for Enhanced Photocatalysis. *Materials* **2023**, *16*, 639. [[CrossRef](#)]
12. Boytsova, O.; Zhukova, I.; Tatarenko, A.; Shatalova, T.; Beiltiukov, A.; Eliseev, A.; Sadovnikov, A. The Anatase-to-Rutile Phase Transition in Highly Oriented Nanoparticles Array of Titania with Photocatalytic Response Changes. *Nanomaterials* **2022**, *12*, 4418. [[CrossRef](#)]
13. Di Paola, A.; Bellardita, M.; Palmisano, L. Brookite, the Least Known TiO₂ Photocatalyst. *Catalysts* **2013**, *3*, 36–73. [[CrossRef](#)]
14. Serga, V.; Burve, R.; Krumina, A.; Romanova, M.; Kotomin, E.A.; Popov, A.I. Extraction–Pyrolytic Method for TiO₂ Polymorphs Production. *Crystals* **2021**, *11*, 431. [[CrossRef](#)]
15. Tsebriienko, T.; Popov, A.I. Effect of Poly (Titanium Oxide) on the Viscoelastic and Thermophysical Properties of Interpenetrating Polymer Networks. *Crystals* **2021**, *11*, 794. [[CrossRef](#)]
16. Trestsova, M.A.; Utepova, I.A.; Chupakhin, O.N.; Semenov, M.V.; Pevtsov, D.N.; Nikolenko, L.M.; Tovstun, S.A.; Gadomska, A.V.; Shchepochkin, A.V.; Kim, G.A.; et al. Oxidative C-H/C-H Coupling of Dipyrromethanes with Azines by TiO₂-Based Photocatalytic System. Synthesis of New BODIPY Dyes and Their Photophysical and Electrochemical Properties. *Molecules* **2021**, *26*, 5549. [[CrossRef](#)]

17. Karawek, A.; Kittipoom, K.; Tansuthepverawongse, L.; Kitjanukit, N.; Neamsung, W.; Lertthanaphol, N.; Chanthara, P.; Ratchahat, S.; Phadungbut, P.; Kim-Lohsoontorn, P.; et al. The Photocatalytic Conversion of Carbon Dioxide to Fuels Using Titanium Dioxide Nanosheets/Graphene Oxide Heterostructure as Photocatalyst. *Nanomaterials* **2023**, *13*, 320. [[CrossRef](#)]
18. Kim, S.-Y.; Lee, T.-G.; Hwangbo, S.-A.; Jeong, J.-R. Effect of the TiO₂ Colloidal Size Distribution on the Degradation of Methylene Blue. *Nanomaterials* **2023**, *13*, 302. [[CrossRef](#)] [[PubMed](#)]
19. Chen, X.; Mao, S.S. Titanium Dioxide Nanomaterials: Synthesis, Properties, Modifications, and Applications. *Chem. Rev.* **2007**, *107*, 2891–2959. [[CrossRef](#)]
20. Dahl, M.; Liu, Y.; Yin, Y. Composite Titanium Dioxide Nanomaterials. *Chem. Rev.* **2014**, *114*, 9853–9889. [[CrossRef](#)]
21. Kumaravel, V.; Mathew, S.; Bartlett, J.; Pillai, S. Photocatalytic hydrogen production using metal doped TiO₂: A review of recent advances. *Appl. Catal. B Environ.* **2019**, *244*, 1021–1064. [[CrossRef](#)]
22. Asahi, R.; Morikawa, T.; Irie, H.; Ohwaki, T. Nitrogen-Doped Titanium Dioxide as Visible-Light-Sensitive Photocatalyst: Designs, Developments, and Prospects. *Chem. Rev.* **2014**, *114*, 9824–9852. [[CrossRef](#)]
23. Wei, L.; Yu, C.; Zhang, Q.; Liu, H.; Wang, Y. TiO₂-based heterojunction photocatalysts for photocatalytic reduction of CO₂ into solar fuels. *J. Mater. Chem. A* **2018**, *6*, 22411–22436. [[CrossRef](#)]
24. Liu, J.; Luo, Z.; Mao, X.; Dong, Y.; Peng, L.; Sun-Waterhouse, D.; Kennedy, J.V.; Waterhouse, G.I.N. Recent Advances in Self-Supported Semiconductor Heterojunction Nanoarrays as Efficient Photoanodes for Photoelectrochemical Water Splitting. *Small* **2022**, *18*, 2204552. [[CrossRef](#)]
25. Chen, X.; Liu, L.; Yu, P.Y.; Mao, S.S. Increasing Solar Absorption for Photocatalysis with Black Hydrogenated Titanium Dioxide Nanocrystals. *Science* **2011**, *331*, 746–750. [[CrossRef](#)]
26. Li, C.; Sun, T.; Zhang, D.; Zhang, X.; Qian, Y.; Zhang, Y.; Lin, X.; Liu, J.; Zhu, L.; Wang, X.; et al. Fabrication of ternary Ag/La-black TiO_{2-x} photocatalyst with enhanced visible-light photocatalytic activity for tetracycline degradation. *J. Alloy. Compd.* **2022**, *891*, 161960. [[CrossRef](#)]
27. Zhu, S.; Yu, Z.; Zhang, L.; Watanabe, S. Solution Plasma-Synthesized Black TiO₂ Nanoparticles for Solar–Thermal Water Evaporation. *ACS Appl. Nano Mater.* **2021**, *4*, 3940–3948. [[CrossRef](#)]
28. Biswas, S.; Lee, H.; Prasad, M.; Sharma, A.; Yu, J.; Sengupta, S.; Deo Pathak, D.; Sinhamahapatra, A. Black TiO_{2-x} Nanoparticles Decorated with Ni Nanoparticles and Trace Amounts of Pt Nanoparticles for Photocatalytic Hydrogen Generation. *ACS Appl. Nano Mater.* **2021**, *4*, 4441–4451. [[CrossRef](#)]
29. Li, Z.; Li, H.; Wang, S.; Yang, F.; Zhou, W. Mesoporous black TiO₂/MoS₂/Cu₂S hierarchical tandem heterojunctions toward optimized photothermal-photocatalytic fuel production. *Chem. Eng. J.* **2022**, *427*, 131830. [[CrossRef](#)]
30. Balati, A.; Tek, S.; Nash, K.; Shipley, H. Nanoarchitecture of TiO₂ microspheres with expanded lattice interlayers and its heterojunction to the laser modified black TiO₂ using pulsed laser ablation in liquid with improved photocatalytic performance under visible light irradiation. *J. Colloid Interface Sci.* **2019**, *541*, 234–248. [[CrossRef](#)]
31. Zhou, L.; Cai, M.; Zhang, X.; Cui, N.; Chen, G.; Zou, G. In-situ nitrogen-doped black TiO₂ with enhanced visible-light-driven photocatalytic inactivation of *Microcystis aeruginosa* cells: Synthesis, performance and mechanism. *Appl. Catal. B Environ.* **2020**, *272*, 119019. [[CrossRef](#)]
32. Zada, I.; Zhang, W.; Sun, P.; Imtiaz, M.; Iqbal, N.; Ghani, U.; Naz, R.; Zhang, Y.; Li, Y.; Gu, J.; et al. Superior photothermal black TiO₂ with random size distribution as flexible film for efficient solar steam generation. *Appl. Mater. Today* **2020**, *20*, 100669. [[CrossRef](#)]
33. Li, F.; Wang, S.; Yin, H.; Chen, Y.; Zhou, Y.; Huang, J.; Ai, S. Photoelectrochemical Biosensor for DNA Formylation Detection in Genomic DNA of Maize Seedlings Based on Black TiO₂-Enhanced Photoactivity of MoS₂/WS₂ Heterojunction. *ACS Sens.* **2020**, *5*, 1092–1101. [[CrossRef](#)]
34. Chen, Y.; Yin, H.; Li, F.; Zhou, J.; Wang, L.; Wang, J.; Ai, S. Polydopamine-sensitized WS₂/black-TiO₂ heterojunction for histone acetyltransferase detection with enhanced visible-light-driven photoelectrochemical activity. *Chem. Eng. J.* **2020**, *393*, 124707. [[CrossRef](#)]
35. Cheng, Y.; Gao, J.; Shi, Q.; Li, Z.; Huang, W. In situ electrochemical reduced Au loaded black TiO₂ nanotubes for visible light photocatalysis. *J. Alloy. Compd.* **2022**, *901*, 163562. [[CrossRef](#)]
36. Touni, A.; Liu, X.; Kang, X.; Carvalho, P.A.; Diplas, S.; Both, K.G.; Sotiropoulos, S.; Chatzitikis, A. Galvanic Deposition of Pt Nanoparticles on Black TiO₂ Nanotubes for Hydrogen Evolving Cathodes. *ChemSusChem* **2021**, *14*, 4993–5003. [[CrossRef](#)] [[PubMed](#)]
37. Lim, J.; Yang, Y.; Hoffmann, M.R. Activation of Peroxymonosulfate by Oxygen Vacancies-Enriched Cobalt-Doped Black TiO₂ Nanotubes for the Removal of Organic Pollutants. *Environ. Sci. Technol.* **2019**, *53*, 6972–6980. [[CrossRef](#)]
38. Qiao, P.; Sun, B.; Li, H.; Pan, K.; Tian, G.; Wang, L.; Zhou, W. Surface Plasmon Resonance-Enhanced Visible-NIR-Driven Photocatalytic and Photothermal Catalytic Performance by Ag/Mesoporous Black TiO₂ Nanotube Heterojunctions. *Chem. Asian J.* **2019**, *14*, 177–186. [[CrossRef](#)]
39. Gao, J.; Xue, J.; Jia, S.; Shen, Q.; Zhang, X.; Jia, H.; Liu, X.; Li, Q.; Wu, L. Self-Doping Surface Oxygen Vacancy-Induced Lattice Strains for Enhancing Visible Light-Driven Photocatalytic H₂ Evolution over Black TiO₂. *ACS Appl. Mater. Interfaces* **2021**, *13*, 18758–18771. [[CrossRef](#)]
40. Shim, Y.; Lim, J.; Hong, S. Black-TiO₂ based photoelectrochemical oxidation of flue-gas desulfurization wastewater for effective reuse in flow-electrode CDI. *Desalination* **2022**, *538*, 115899. [[CrossRef](#)]

41. Chen, J.; Fu, Y.; Sun, F.; Hu, Z.; Wang, X.; Zhang, T.; Zhang, F.; Wu, X.; Chen, H.; Cheng, G.; et al. Oxygen vacancies and phase tuning of self-supported black TiO_{2-x} nanotube arrays for enhanced sodium storage. *Chem. Eng. J.* **2020**, *400*, 125784. [[CrossRef](#)]
42. Gao, J.; Shen, Q.; Guan, R.; Xue, J.; Liu, X.; Jia, H.; Li, Q.; Wu, Y. Oxygen vacancy self-doped black TiO₂ nanotube arrays by aluminothermic reduction for photocatalytic CO₂ reduction under visible light illumination. *J. CO₂ Util.* **2020**, *35*, 205–215. [[CrossRef](#)]
43. Li, Z.; Bian, H.; Xiao, X.; Shen, J.; Zhao, C.; Lu, J.; Li, Y. Defective Black TiO₂ Nanotube Arrays for Enhanced Photocatalytic and Photoelectrochemical Applications. *ACS Appl. Nano Mater.* **2019**, *2*, 7372–7378. [[CrossRef](#)]
44. Zhang, D.; Cong, T.; Xia, L.; Pan, L. Growth of black TiO₂ nanowire/carbon fiber composites with dendritic structure for efficient visible-light-driven photocatalytic degradation of methylene blue. *J. Mater. Sci.* **2019**, *54*, 7576–7588. [[CrossRef](#)]
45. Yang, L.; Peng, Y.; Yang, Y.; Liu, J.; Li, Z.; Ma, Y.; Zhang, Z.; Wei, Y.; Li, S.; Huang, Z.; et al. Green and Sensitive Flexible Semiconductor SERS Substrates: Hydrogenated Black TiO₂ Nanowires. *ACS Appl. Nano Mater.* **2018**, *1*, 4516–4527. [[CrossRef](#)]
46. Nawaz, R.; Sahrin, N.T.; Haider, S.; Ullah, H.; Junaid, M.; Akhtar, M.S.; Khan, S. Photocatalytic performance of black titanium dioxide for phenolic compounds removal from oil refinery wastewater: Nanoparticles vs. nanowires. *Appl. Nanosci.* **2022**, *12*, 3499–3515. [[CrossRef](#)]
47. Lim, J.; Kim, S.; Armengol, R.A.; Kasian, O.; Choi, P.; Stephenson, L.T.; Gault, B.; Scheu, C. Atomic-Scale Mapping of Impurities in Partially Reduced Hollow TiO₂ Nanowires. *Angew. Chem. Int. Ed.* **2020**, *59*, 5651–5655. [[CrossRef](#)]
48. Xue, X.; Chen, H.; Xiong, Y.; Chen, R.; Jiang, M.; Fu, G.; Xi, Z.; Zhang, X.; Ma, J.; Fang, W.; et al. Near-Infrared-Responsive Photo-Driven Nitrogen Fixation Enabled by Oxygen Vacancies and Sulfur Doping in Black TiO_{2-x}S_y Nanoplatelets. *ACS Appl. Mater. Interfaces* **2021**, *13*, 4975–4983. [[CrossRef](#)]
49. Sun, L.; Xie, J.; Zhang, L.; Jiang, R.; Wu, J.; Fan, L.; Shao, R.; Chen, Z.; Jin, Z. 2D black TiO_{2-x} nanoplate-decorated Ti₃C₂ MXene hybrids for ultrafast and elevated stable lithium storage. *FlatChem* **2020**, *20*, 100152. [[CrossRef](#)]
50. Zhu, G.; Ma, L.; Lin, H.; Zhao, P.; Wang, L.; Hu, Y.; Chen, R.; Chen, T.; Wang, Y.; Tie, Z.; et al. High-performance Li-ion capacitor based on black-TiO_{2-x}/graphene aerogel anode and biomass-derived microporous carbon cathode. *Nano Res.* **2019**, *12*, 1713–1719. [[CrossRef](#)]
51. Zhang, W.; Xue, J.; Shen, Q.; Jia, S.; Gao, J.; Liu, X.; Jia, H. Black single-crystal TiO₂ nanosheet array films with oxygen vacancy on {001} facets for boosting photocatalytic CO₂ reduction. *J. Alloys Compd.* **2021**, *870*, 159400. [[CrossRef](#)]
52. Zou, L.; Zhu, Y.; Hu, Z.; Cao, X.; Cen, W. Remarkably improved photocatalytic hydrogen evolution performance of crystalline TiO₂ nanobelts hydrogenated at atmospheric pressure with the assistance of hydrogen spillover. *Catal. Sci. Technol.* **2022**, *12*, 5575–5585. [[CrossRef](#)]
53. Zhang, T.; Xing, Z.; Xiu, Z.; Li, Z.; Yang, S.; Zhu, Q.; Zhou, W. Surface defect and rational design of TiO_{2-x} nanobelts/ g-C₃N₄ nanosheets/ CdS quantum dots hierarchical structure for enhanced visible-light-driven photocatalysis. *Int. J. Hydrog. Energ.* **2019**, *44*, 1586–1596.
54. Zhao, Q.; Bi, R.; Cui, J.; Yang, X.; Zhang, L. TiO_{2-x} Nanocages Anchored in N-Doped Carbon Fiber Films as a Flexible Anode for High-Energy Sodium-Ion Batteries. *ACS Appl. Energy Mater.* **2018**, *1*, 4459–4466. [[CrossRef](#)]
55. Yu, Z.; Xun, S.; Jing, M.; Chen, H.; Song, W.; Chao, Y.; Rahmani, M.; Ding, Y.; Hua, M.; Liu, J.; et al. Construction of 3D TiO₂ nanoflower for deep catalytic oxidative desulfurization in diesel: Role of oxygen vacancy and Ti³⁺. *J. Hazard. Mater.* **2022**, *440*, 129859. [[CrossRef](#)]
56. Choi, J.U.; Kim, Y.G.; Jo, W.K. Multiple photocatalytic applications of non-precious Cu-loaded g-C₃N₄/hydrogenated black TiO₂ nanofiber heterostructure. *Appl. Surf. Sci.* **2019**, *473*, 761–769. [[CrossRef](#)]
57. Yan, Z.; Huang, W.; Jiang, X.; Gao, J.; Hu, Y.; Zhang, H.; Shi, Q. Hollow structured black TiO₂ with thickness-controllable microporous shells for enhanced visible-light-driven photocatalysis. *Microporous Mesoporous Mater.* **2021**, *323*, 111228. [[CrossRef](#)]
58. Shi, X.; Liu, Z.; Li, X.; You, W.; Shao, Z.; Che, R. Enhanced dielectric polarization from disorder-engineered Fe₃O₄@black TiO_{2-x} heterostructure for broadband microwave absorption. *Chem. Eng. J.* **2021**, *419*, 130020. [[CrossRef](#)]
59. Ren, L.; Zhou, W.; Sun, B.; Li, H.; Qiao, P.; Xu, Y.; Wu, J.; Lin, K.; Fu, H. Defects-engineering of magnetic γ-Fe₂O₃ ultra-thin nanosheets/mesoporous black TiO₂ hollow sphere heterojunctions for efficient charge separation and the solar-driven photocatalytic mechanism of tetracycline degradation. *Appl. Catal. B Environ.* **2019**, *240*, 319–328. [[CrossRef](#)]
60. Varnagiris, S.; Medvids, A.; Lelis, M.; Milcius, D.; Antuzevics, A. Black carbon-doped TiO₂ films: Synthesis, characterization and photocatalysis. *J. Photochem. Photobiol. A Chem.* **2019**, *382*, 111941. [[CrossRef](#)]
61. Islam, S.Z.; Reed, A.; Nagpure, S.; Wanninayake, N.; Browning, J.F.; Strzalka, J.; Kim, D.Y.; Rankin, S.E. Hydrogen incorporation by plasma treatment gives mesoporous black TiO₂ thin films with visible photoelectrochemical water oxidation activity. *Microporous Mesoporous Mater.* **2018**, *261*, 35–43. [[CrossRef](#)]
62. Chahrouh, K.M.; Yam, F.K.; Eid, A.M.; Nazeer, A.A. Enhanced photoelectrochemical properties of hierarchical black TiO_{2-x} nanolaces for Cr (VI) photocatalytic reduction. *Int. J. Hydrog. Energ.* **2020**, *45*, 22674–22690. [[CrossRef](#)]
63. Katal, R.; Salehi, M.; Hossein, M.; Farahani, D.A.; Masudy-Panah, S.; Ong, S.L.; Hu, J. Preparation of a New Type of Black TiO₂ under a Vacuum Atmosphere for Sunlight Photocatalysis. *ACS Appl. Mater. Interfaces* **2018**, *10*, 35316–35326. [[CrossRef](#)] [[PubMed](#)]
64. Hu, W.; Zhou, W.; Zhang, K.; Zhang, X.; Wang, L.; Jiang, B.; Tian, G.; Zhao, D.; Fu, H. Facile strategy for controllable synthesis of stable mesoporous black TiO₂ hollow spheres with efficient solar-driven photocatalytic hydrogen evolution. *J. Mater. Chem. A* **2016**, *4*, 7495–7502. [[CrossRef](#)]

65. Zhang, K.; Zhou, W.; Zhang, X.; Sun, B.; Wang, L.; Pan, K.; Jiang, B.; Tian, G.; Fu, H. Self-floating amphiphilic black TiO₂ foams with 3D macro-mesoporous architectures as efficient solar-driven photocatalysts. *Appl. Catal. B Environ.* **2017**, *206*, 336–343. [[CrossRef](#)]
66. Zhou, G.; Meng, H.; Cao, Y.; Kou, X.; Duan, S.; Fan, L.; Xiao, M.; Zhou, F.; Li, Z.; Xing, Z. Surface plasmon resonance-enhanced solar-driven photocatalytic performance from Ag nanoparticles-decorated Ti³⁺ self-doped porous black TiO₂ pillars. *J. Ind. Eng. Chem.* **2018**, *64*, 188–193. [[CrossRef](#)]
67. Kang, J.; Zhang, Y.; Chai, Z.; Qiu, X.; Cao, X.; Zhang, P.; Teobaldi, G.; Liu, L.; Guo, L. Amorphous Domains in Black Titanium Dioxide. *Adv. Matter.* **2021**, *33*, 2100407. [[CrossRef](#)]
68. Ullattil, S.G.; Narendranth, S.B.; Pillai, S.C.; Periyat, P. Black TiO₂ Nanomaterials: A Review of Recent Advances. *Chem. Eng. J.* **2018**, *343*, 708–736. [[CrossRef](#)]
69. Zheng, P.; Zhang, L.; Zhang, X.; Ma, Y.; Qian, J.; Jiang, Y.; Li, H. Hydrogenation of TiO₂ nanosheets and nanoparticles: Typical reduction stages and orientation-related anisotropic disorder. *J. Mater. Chem. A* **2021**, *9*, 22603–22614. [[CrossRef](#)]
70. Ioannidou, E.; Ioannidi, A.; Frontistis, Z.; Antonopoulou, M.; Tselios, C.; Tsikritzis, D.; Konstantinou, I.; Kennou, S.; Kondarides, D.I.; Mantzavinos, D. Correlating the properties of hydrogenated titania to reaction kinetics and mechanism for the photocatalytic degradation of bisphenol A under solar irradiation. *Appl. Catal. B Environ.* **2016**, *188*, 65–76. [[CrossRef](#)]
71. Koohgard, M.; Hosseini-Sarvari, M. Black TiO₂ nanoparticles with efficient photocatalytic activity under visible light at low temperature: Regioselective C-N bond cleavage toward the synthesis of thioureas, sulfonamides, and propargylamines. *Catal. Sci. Technol.* **2020**, *10*, 6825–6839. [[CrossRef](#)]
72. Andronic, L.; Enesca, A. Black TiO₂ Synthesis by Chemical Reduction Methods for Photocatalysis Applications. *Front. Chem.* **2020**, *8*, 565489. [[CrossRef](#)]
73. Wang, X.; Mayrhofer, L.; Hofer, M.; Estrade, S.; Lopez-Conesa, L.; Zhou, H.; Lin, Y.; Peiró, F.; Fan, Z.; Shen, H.; et al. Facile and Efficient Atomic Hydrogenation Enabled Black TiO₂ with Enhanced Photo-Electrochemical Activity via a Favorably Low-Energy-Barrier Pathway. *Adv. Energy Mater.* **2019**, *9*, 1900725. [[CrossRef](#)]
74. Zimbone, M.; Cacciato, G.; Sanz, R.; Carles, R.; Gulino, A.; Privitera, V.; Grimaldi, M.G. Black TiO_x photocatalyst obtained by laser irradiation in water. *Catal. Commun.* **2016**, *84*, 11–15. [[CrossRef](#)]
75. Yao, D.; Hu, Z.; Zheng, L.; Chen, S.; Lü, W.; Xu, H. Laser-engineered black rutile TiO₂ photoanode for CdS/CdSe-sensitized quantum dot solar cells with a significant power conversion efficiency of 9.1%. *Appl. Surf. Sci.* **2023**, *608*, 155230. [[CrossRef](#)]
76. Dong, J.; Han, J.; Liu, Y.; Nakajima, A.; Matsushita, S.; Wei, S.; Gao, W. Defective Black TiO₂ Synthesized via Anodization for Visible-Light Photocatalysis. *ACS Appl. Mater. Interfaces* **2014**, *6*, 1385–1388. [[CrossRef](#)]
77. Teng, F.; Li, M.; Gao, C.; Zhang, G.; Zhang, P.; Wang, Y.; Chen, L.; Xie, E. Preparation of black TiO₂ by hydrogen plasma assisted chemical vapor deposition and its photocatalytic activity. *Appl. Catal. B Environ.* **2014**, *148–149*, 339–343. [[CrossRef](#)]
78. Huang, H.; Zhang, H.; Ma, Z.; Liu, Y.; Zhang, X.; Han, Y.; Kang, Z. Si quantum dot-assisted synthesis of mesoporous black TiO₂ nanocrystals with high photocatalytic activity. *J. Mater. Chem. A* **2013**, *1*, 4162–4166. [[CrossRef](#)]
79. Zhou, W.; Li, W.; Wang, J.; Qu, Y.; Yang, Y.; Xie, Y.; Zhang, K.; Wang, L.; Fu, H.; Zhao, D. Ordered Mesoporous Black TiO₂ as Highly Efficient Hydrogen Evolution Photocatalyst. *J. Am. Chem. Soc.* **2014**, *136*, 9280–9283. [[CrossRef](#)]
80. Yang, W.; Li, M.; Pan, K.; Guo, L.; Wu, J.; Li, Z.; Yang, F.; Lin, K.; Zhou, W. Surface engineering of mesoporous anatase titanium dioxide nanotubes for rapid spatial charge separation on horizontal-vertical dimensions and efficient solar-driven photocatalytic hydrogen evolution. *J. Colloid Interface Sci.* **2021**, *586*, 75–83. [[CrossRef](#)]
81. Li, Z.; Wang, S.; Xie, Y.; Yang, W.; Tao, B.; Lu, J.; Wu, J.; Qu, Y.; Zhou, W. Surface defects induced charge imbalance for boosting charge separation and solar-driven photocatalytic hydrogen evolution. *J. Colloid Interface Sci.* **2021**, *596*, 12–21. [[CrossRef](#)] [[PubMed](#)]
82. Zhang, X.; Hu, W.; Zhang, K.; Wang, J.; Sun, B.; Li, H.; Qiao, P.; Wang, L.; Zhou, W. Ti³⁺ Self-Doped Black TiO₂ Nanotubes with Mesoporous Nanosheet Architecture as Efficient Solar-Driven Hydrogen Evolution Photocatalysts. *ACS Sustain. Chem. Eng.* **2017**, *5*, 6894–6901. [[CrossRef](#)]
83. Wu, J.; Qiao, P.; Li, H.; Xu, Y.; Yang, W.; Yang, F.; Lin, K.; Pan, K.; Zhou, W. Engineering surface defects on two-dimensional ultrathin mesoporous anatase TiO₂ nanosheets for efficient charge separation and exceptional solar-driven photocatalytic hydrogen evolution. *J. Mater. Chem. C* **2020**, *8*, 3476–3482. [[CrossRef](#)]
84. Wu, S.; Li, X.; Tian, Y.; Lin, Y.; Hu, Y.H. Excellent photocatalytic degradation of tetracycline over black anatase-TiO₂ under visible light. *Chem. Eng. J.* **2021**, *406*, 126747. [[CrossRef](#)]
85. Hamad, H.; Bailón-García, E.; Maldonado-Hódar, F.J.; Pérez-Cadenas, A.F.; Carrasco-Marín, F.; Morales-Torres, S. Synthesis of Ti_xO_y nanocrystals in mild synthesis conditions for the degradation of pollutants under solar light. *Appl. Catal. B Environ.* **2019**, *241*, 385–392. [[CrossRef](#)]
86. Cai, J.; Wu, M.; Wang, Y.; Zhang, H.; Meng, M.; Tian, Y.; Li, X.; Zhang, J.; Zheng, L.; Gong, J. Synergetic Enhancement of Light Harvesting and Charge Separation over Surface-Disorder-Engineered TiO₂ Photonic Crystals. *Chem* **2017**, *2*, 877–892. [[CrossRef](#)]
87. Xiao, F.; Zhou, W.; Sun, B.; Li, H.; Qiao, P.; Ren, L.; Zhao, X.; Fu, H. Engineering oxygen vacancy on rutile TiO₂ for efficient electron-hole separation and high solar-driven photocatalytic hydrogen evolution. *Sci. China Mater.* **2018**, *61*, 822–830. [[CrossRef](#)]
88. Zhu, G.; Yin, H.; Yang, C.; Cui, H.; Wang, Z.; Xu, J.; Lin, T.; Huang, F. Black Titania for Superior Photocatalytic Hydrogen Production and Photoelectrochemical Water Splitting. *ChemCatChem* **2015**, *7*, 2614–2619. [[CrossRef](#)]

89. Sinhamahapatra, A.; Jeon, J.P.; Yu, J.S. A new approach to prepare highly active and stable black titania for visible light-assisted hydrogen production. *Energy Environ. Sci.* **2015**, *8*, 3539–3544. [[CrossRef](#)]
90. Ullattil, S.G.; Periyat, P. A 'one pot' gel combustion strategy towards Ti³⁺ self-doped 'black' anatase TiO_{2-x} solar photocatalyst. *J. Mater. Chem. A* **2016**, *4*, 5854–5858. [[CrossRef](#)]
91. Campbell, L.; Nguyen, S.H.; Webb, H.K.; Eldridge, D.S. Photocatalytic disinfection of *S. aureus* using black TiO_{2-x} under visible light. *Catal. Sci. Technol.* **2023**, *13*, 62–71. [[CrossRef](#)]
92. Basavarajappa, P.S.; Patil, S.B.; Ganganagappa, N.; Reddy, K.R.; Raghu, A.V.; Reddy, C.V. Recent progress in metal-doped TiO₂, non-metal doped/codoped TiO₂ and TiO₂ nanostructured hybrids for enhanced photocatalysis. *Int. J. Hydrog. Energy* **2020**, *45*, 7764–7778. [[CrossRef](#)]
93. Nah, Y.C.; Paramasivam, I.; Schmuki, P. Doped TiO₂ and TiO₂ Nanotubes: Synthesis and Applications. *ChemPhysChem* **2010**, *11*, 2698–2713. [[CrossRef](#)]
94. Yi, L.; Ci, S.; Luo, S.; Shao, P.; Hou, Y.; Wen, Z. Scalable and low-cost synthesis of black amorphous Al-Ti-O nanostructure for high-efficient photothermal desalination. *Nano Energy* **2017**, *41*, 600–608. [[CrossRef](#)]
95. Zhang, H.; Xing, Z.; Zhang, Y.; Li, Z.; Wu, X.; Liu, C.; Zhu, Q.; Zhou, W. Ni²⁺ and Ti³⁺ co-doped porous black anatase TiO₂ with unprecedented-high visible-light-driven photocatalytic degradation performance. *RSC Adv.* **2015**, *5*, 107150–107157. [[CrossRef](#)]
96. Ansari, S.A.; Khan, M.M.; Ansari, M.O.; Cho, M.H. Nitrogen-doped titanium dioxide (N-doped TiO₂) for visible light photocatalysis. *New J. Chem.* **2016**, *40*, 3000–3009. [[CrossRef](#)]
97. Petala, A.; Tsikritzis, D.; Kollia, M.; Ladas, S.; Kennou, S.; Kondarides, D.I. Synthesis and characterization of N-doped TiO₂ photocatalysts with tunable response to solar radiation. *Appl. Surf. Sci.* **2014**, *305*, 281–291. [[CrossRef](#)]
98. Asahi, R.; Morikawa, T.; Ohwaki, T.; Aoki, K.; Taga, Y. Visible-Light Photocatalysis in Nitrogen-Doped Titanium Oxides. *Science* **2001**, *293*, 269–271. [[CrossRef](#)]
99. Hu, Z.; Xu, T.; Liu, P.; Oeser, M. Microstructures and optical performances of nitrogen-vanadium co-doped TiO₂ with enhanced purification efficiency to vehicle exhaust. *Environ. Res.* **2021**, *193*, 110560. [[CrossRef](#)]
100. Liu, H.; Fan, H.; Wu, R.; Tian, L.; Yang, X.; Sun, Y. Nitrogen-doped black TiO₂ spheres with enhanced visible light photocatalytic performance. *SN Appl. Sci.* **2019**, *1*, 487. [[CrossRef](#)]
101. Gao, J.; Xue, J.; Shen, Q.; Liu, T.; Zhang, X.; Liu, X.; Jia, H.; Li, Q.; Wu, Y. A promoted photocatalysis system trade-off between thermodynamic and kinetic via hierarchical distribution dual-defects for efficient H₂ evolution. *Chem. Eng. J.* **2022**, *431*, 133281. [[CrossRef](#)]
102. Cao, Y.; Xing, Z.; Hu, M.; Li, Z.; Wu, X.; Zhao, T.; Xiu, Z.; Yang, S.; Zhou, W. Mesoporous black N-TiO_{2-x} hollow spheres as efficient visible-light-driven photocatalysts. *J. Catal.* **2017**, *356*, 246–254. [[CrossRef](#)]
103. Wang, S.; Gao, Y.; Miao, S.; Liu, T.; Li, R.; Mu, L.; Li, R.; Fan, F.; Li, C. Positioning the Water Oxidation Reaction Sites in Plasmonic Photocatalysts. *J. Am. Chem. Soc.* **2017**, *139*, 11771–11778. [[CrossRef](#)]
104. Jiang, J.; Xing, Z.; Li, M.; Li, Z.; Yin, J.; Kuang, J.; Zou, J.; Zhu, Q.; Zhou, W. Plasmon Ag decorated 3D urchinlike N-TiO_{2-x} for enhanced visible-light-driven photocatalytic performance. *J. Colloid Interface Sci.* **2018**, *521*, 102–110. [[CrossRef](#)] [[PubMed](#)]
105. Li, H.; Shen, L.; Zhang, K.; Sun, B.; Ren, L.; Qiao, P.; Pan, K.; Wang, L.; Zhou, W. Surface plasmon resonance-enhanced solar-driven photocatalytic performance from Ag nanoparticle-decorated self-floating porous black TiO₂ foams. *Appl. Catal. B: Environ.* **2018**, *220*, 111–117. [[CrossRef](#)]
106. Kuang, J.; Xing, Z.; Yin, J.; Li, Z.; Zhu, Q.; Zhou, W. Surface plasma Ag-decorated single-crystalline TiO_{2-x}(B) nanorod/defect-rich g-C₃N₄ nanosheet ternary superstructure 3D heterojunctions as enhanced visible-light-driven photocatalyst. *J. Colloid Interface Sci.* **2019**, *542*, 63–72. [[CrossRef](#)]
107. Li, M.; Xing, Z.; Jiang, J.; Li, Z.; Yin, J.; Kuang, J.; Tan, S.; Zhu, Q.; Zhou, W. Surface plasmon resonance-enhanced visible-light-driven photocatalysis by Ag nanoparticles decorated S-TiO_{2-x} nanorods. *J. Taiwan Inst. Chem. Eng.* **2018**, *82*, 198–204. [[CrossRef](#)]
108. Xiao, Y.; Wang, K.; Yang, Z.; Xing, Z.; Li, Z.; Pan, K.; Zhou, W. Plasma Cu-decorated TiO_{2-x}/CoP particle-level hierarchical heterojunctions with enhanced photocatalytic-photothermal performance. *J. Hazard. Mater.* **2021**, *414*, 125487. [[CrossRef](#)]
109. Wang, S.; Sun, H.; Qiao, P.; Li, Z.; Xie, Y.; Zhou, W. NiS/Pt nanoparticles co-decorated black mesoporous TiO₂ hollow nanotube assemblies as efficient hydrogen evolution photocatalysts. *Appl. Mater. Today* **2021**, *22*, 100977. [[CrossRef](#)]
110. Wang, C.; Li, J.; Paineau, E.; Remita, H.; Ghazzal, M.N. Pt Atomically Dispersed in Black TiO_{2-x}/CuxO with Chiral-Like Nanostructure for Visible-Light H₂ Generation. *Sol. RRL* **2023**, 2200929, early view. [[CrossRef](#)]
111. Yin, J.; Xing, Z.; Kuang, J.; Li, Z.; Zhu, Q.; Zhou, W. Dual oxygen vacancy defects-mediated efficient electron-hole separation via surface engineering of Ag/Bi₂MoO₆ nanosheets/TiO₂ nanobelts ternary heterostructures. *J. Ind. Eng. Chem.* **2019**, *78*, 155–163. [[CrossRef](#)]
112. Liu, X.; Xing, Z.; Zhang, Y.; Li, Z.; Wu, X.; Tan, S.; Yu, X.; Zhu, Q.; Zhou, W. Fabrication of 3D flower-like black N-TiO_{2-x}@MoS₂ for unprecedented-high visible-light-driven photocatalytic performance. *Appl. Catal. B Environ.* **2017**, *201*, 119–127. [[CrossRef](#)]
113. Shen, L.; Xing, Z.; Zou, J.; Li, Z.; Wu, X.; Zhang, Y.; Zhu, Q.; Yang, S.; Zhou, W. Black TiO₂ nanobelts/g-C₃N₄ nanosheets Laminated Heterojunctions with Efficient Visible-Light-Driven Photocatalytic Performance. *Sci. Rep.* **2017**, *7*, 41978. [[CrossRef](#)]
114. Hu, M.; Xing, Z.; Cao, Y.; Li, Z.; Yan, X.; Xiu, Z.; Zhao, T.; Yang, S.; Zhou, W. Ti³⁺ self-doped mesoporous black TiO₂/SiO₂/g-C₃N₄ sheets heterojunctions as remarkable visible-light-driven photocatalysts. *Appl. Catal. B Environ.* **2018**, *226*, 499–508. [[CrossRef](#)]

115. Zhao, T.; Xing, Z.; Xiu, Z.; Li, Z.; Shen, L.; Cao, Y.; Hu, M.; Yang, S.; Zhou, W. CdS quantum dots/Ti³⁺-TiO₂ nanobelts heterojunctions as efficient visible-light-driven photocatalysts. *Mater. Res. Bull.* **2018**, *103*, 114–121. [[CrossRef](#)]
116. Sun, B.; Zhou, W.; Li, H.; Ren, L.; Qiao, P.; Xiao, F.; Wang, L.; Jiang, B.; Fu, H. Magnetic Fe₂O₃/mesoporous black TiO₂ hollow sphere heterojunctions with wide-spectrum response and magnetic separation. *Appl. Catal. B Environ.* **2018**, *221*, 235–242. [[CrossRef](#)]
117. Xiu, Z.; Xing, Z.; Li, Z.; Wu, X.; Yan, X.; Hu, M.; Cao, Y.; Yang, S.; Zhou, W. Ti³⁺-TiO₂/Ce³⁺-CeO₂ Nanosheet heterojunctions as efficient visible-light-driven photocatalysts. *Mater. Res. Bull.* **2018**, *100*, 191–197. [[CrossRef](#)]
118. Tan, S.; Xing, Z.; Zhang, J.; Li, Z.; Wu, X.; Cui, J.; Kuang, J.; Zhu, Q.; Zhou, W. Ti³⁺-TiO₂/g-C₃N₄ mesostructured nanosheets heterojunctions as efficient visible-light-driven photocatalysts. *J. Catal.* **2018**, *357*, 90–99. [[CrossRef](#)]
119. Kuang, J.; Xing, Z.; Yin, J.; Li, Z.; Zhu, Q.; Zhou, W. Assembly of surface-defect single-crystalline strontium titanate nanocubes acting as molecular bricks onto surface-defect single-crystalline titanium dioxide (B) nanorods for efficient visible-light-driven photocatalytic performance. *J. Colloid Interface Sci.* **2019**, *537*, 441–449. [[CrossRef](#)]
120. Sun, D.; Chi, D.; Yang, Z.; Xing, Z.; Chen, P.; Li, Z.; Pan, K.; Zhou, W. CdS quantum dots modified surface oxygen vacancy defect ZnO_{1-x}-TiO_{2-x} solid solution sphere as Z-Scheme heterojunctions for efficient visible light-driven photothermal-photocatalytic performance. *J. Alloys Compd.* **2020**, *826*, 154218. [[CrossRef](#)]
121. Liu, X.; Xing, Z.; Zhang, H.; Wang, W.; Zhang, Y.; Li, Z.; Wu, X.; Yu, X.; Zhou, W. Fabrication of 3D Mesoporous Black TiO₂/MoS₂/TiO₂ Nanosheets for Visible-Light-Driven Photocatalysis. *ChemSusChem* **2016**, *9*, 1118–1124. [[CrossRef](#)]
122. Sun, B.; Zhou, W.; Li, H.; Ren, L.; Qiao, P.; Li, W.; Fu, H. Synthesis of Particulate Hierarchical Tandem Heterojunctions toward Optimized Photocatalytic Hydrogen Production. *Adv. Mater.* **2018**, *30*, 1804282. [[CrossRef](#)]
123. Zhang, K.; Zhou, W.; Zhang, X.; Qu, Y.; Wang, L.; Hu, W.; Pan, K.; Li, M.; Xie, Y.; Jiang, B.; et al. Large-scale synthesis of stable mesoporous black TiO₂ nanosheets for efficient solar-driven photocatalytic hydrogen evolution via an earth-abundant low-cost biotemplate. *RSC Adv.* **2016**, *6*, 50506–50512. [[CrossRef](#)]
124. Lee, B.T.; Han, J.K.; Gain, A.K.; Lee, K.H.; Saito, F. TEM microstructure characterization of nano TiO₂ coated on nano ZrO₂ powders and their photocatalytic activity. *Mater. Lett.* **2006**, *60*, 2101–2104. [[CrossRef](#)]
125. Wafi, M.A.E.; Ahmed, M.A.; Abdel-Samad, H.S.; Medien, H.A.A. Exceptional removal of methylene blue and p-aminophenol dye over novel TiO₂/RGO nanocomposites by tandem adsorption-photocatalytic processes. *Mater. Sci. Energy Technol.* **2022**, *5*, 217–231. [[CrossRef](#)]
126. Zeshan, M.; Bhatti, I.A.; Mohsin, M.; Iqbal, M.; Amjed, N.; Nisar, J.; AlMasoud, N.; Alomar, T.S. Remediation of pesticides using TiO₂ based photocatalytic strategies: A review. *Chemosphere* **2022**, *300*, 134525. [[CrossRef](#)]
127. Jiang, X.; Fuji, M. In-Situ Preparation of Black TiO₂/Cu₂O/Cu Composites as an Efficient Photocatalyst for Degradation Pollutants and Hydrogen Production. *Catal. Lett.* **2022**, *152*, 3272–3283. [[CrossRef](#)]
128. Qiang, C.; Li, N.; Zuo, S.; Guo, Z.; Zhan, W.; Li, Z.; Ma, J. Microwave-assisted synthesis of RuTe₂/black TiO₂ photocatalyst for enhanced diclofenac degradation: Performance, mechanistic investigation and intermediates analysis. *Sep. Purif. Technol.* **2022**, *283*, 120214. [[CrossRef](#)]

Disclaimer/Publisher's Note: The statements, opinions and data contained in all publications are solely those of the individual author(s) and contributor(s) and not of MDPI and/or the editor(s). MDPI and/or the editor(s) disclaim responsibility for any injury to people or property resulting from any ideas, methods, instructions or products referred to in the content.